Geophys. J. Int. (1995) **120**, 111–131

Coincident conductive and reflective middle and lower crust in southern British Columbia

Guy Marquis,[1,*] Alan G. Jones[2] and Roy D. Hyndman[1,3]

[1]*School of Earth and Ocean Sciences, University of Victoria, Victoria, BC, Canada,* V8W 2Y2
[2]*Geological Survey of Canada, 1 Observatory Crescent, Ottawa, Ont, Canada,* K1A 0Y3
[3]*Pacific Geoscience Centre, Geological Survey of Canada, Sidney, BC, Canada,* V8L 4B2

Accepted 1994 June 16. Received 1994 June 16; in original form 1993 May 4

SUMMARY

Processing and interpretation of magnetotelluric data, recorded as part of the LITHOPROBE Southern Cordillera transect studies, across the boundary of the Intermontane and Omineca morphogeological belts reveals: (a) high electrical conductivity in the middle and lower parts of the crust everywhere, and (b) a depth dependency of geoelectric strike. The data have been modelled using two different inversion algorithms and different methods for correcting 'static shifts'. The two different approaches gave similar results: the depth to the top of a conductive layer decreases from 15–17 km in the west across the Intermontane Belt to 8–10 km across the transition to the Omineca Belt. The top of this conductive layer is closely coincident with a layer of increased seismic reflectivity as shown by reprocessing of collocated LITHOPROBE seismic-reflection data. The eastward shallowing is associated with an increase in heat flow such that the top of the conductive and reflective zones remains at 400–450 °C. This coincidence suggests that the increased reflectivity and the high electrical conductivity observed in the middle crust may have a common cause, and that their presence is limited to where the present temperature exceeds a critical value. One explanation that meets these conditions is that both the conductivity and reflectivity are produced by a small amount of aqueous fluid porosity. We propose that fluids are trapped in the middle crust by a ductile shear zone, previously interpreted from the seismic sections as the Okanagan Valley Fault to the west of Okanagan lake. The geoelectrical strike varies from N25°W for the first 5–10 km of the crust, to N20°E for the middle/lower crust, and to N60°E for the upper mantle. This variation indicates that the exotic terrane material is concentrated in the uppermost part of the crust and that the remainder of the crust is composed of ancestral North American rocks.

Key words: Canadian Cordillera, deep crustal conductors, heat flow, porosity, reflectors.

INTRODUCTION

The southern Canadian Cordillera is divided into a series of subparallel morphogeological belts representing oceanic and island arc terranes accreted to the North American Craton in the Mesozoic (e.g. Gabrielse & Yorath 1991). The boundary of interest in this article is that between the Intermontane and Omineca Belts. The Omineca Belt is bounded on the east by the Foreland Belt consisting of rocks thrust over the North American Craton, whereas the Intermontane Belt is bounded on the west by the Coast Crystalline Belt and is physiographically subdued. Volcanic and sedimentary rocks, usually subject to little metamorphism, are widespread in the Intermontane Belt. This belt contains most of the components of the Intermontane Superterrane accreted in the Mesozoic (e.g. Irving & Wynne 1991). The Omineca Belt is an uplifted region extensively underlain by metamorphic and granitic rocks that straddle the boundary between the accreted terranes and ancestral

* Now at: Ecole et Observatoire de Physique du Gldoe, 5 rue René Descartes, 67084 Strasbourg Cedex, France.

North America. In the area of this study its western boundary with the Intermontane Belt is the western limit of the metamorphic and granitic rocks of the Shuswap metamorphic complex. The Intermontane–Omineca boundary approximately corresponds to the present line between $^{87}Sr/^{86}Sr$ of 0.704, with the higher values to the east associated with older continental basement and the lower values to the west associated with the accreted oceanic terranes. An important feature for the structure and for the thermal regime is that the Omineca Belt has undergone Early Tertiary extension, uplift and erosion, whereas most of the Intermontane Belt has not.

Global compilations of nearly coincident geophysical data suggest an intriguing correlation between deep crustal conductivity, crustal reflectivity and the thermal regime, especially in Phanerozoic regions (Hyndman & Shearer 1989; Marquis & Hyndman 1992). High conductivity and general subhorizontal reflectivity commonly occur in the lower crust where the present temperature exceeds 400–450°C (Gough 1986b; Jones 1987, 1992; Marquis & Hyndman 1992). Whilst these characteristics of the lower crust have many possible explanations, a small aqueous porosity (0.5–1.5 per cent) can explain them all (Marquis & Hyndman 1992). However, few of the studies reported in the literature have been optimal for comparison of different data types. Correlations usually depend upon electromagnetic and seismic surveys of the same tectonic unit made at different localities, sometimes separated by many tens of kilometres. The multidisciplinary LITHOPROBE Southern Cordillera transect investigations provide an excellent opportunity to interpret jointly coincident high-quality deep crustal geophysical data. In addition to the primary program of reflection seismic profiling, extensive magnetotelluric and seismic refraction surveys were undertaken, and regional geothermal data have been obtained.

This paper deals mostly with the analysis of LITHOPROBE magnetotelluric and associated reflection data from profiles extending from the Intermontane Belt to the Omineca Belt in southern British Columbia (Fig. 1). The MT data are corrected for galvanic distortion, and the spatial variation of geoelectric strike with increasing period, equivalent to increasing depth, is derived. The data are modelled in the regional strike frame appropriate for the bulk of the crust

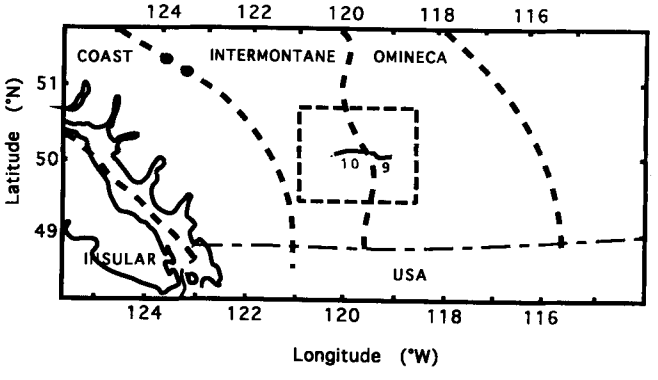

Figure 1. General map of the southern Canadian Cordillera and location of LITHOPROBE Lines 9 and 10. The major morphological belts are identified in upper case letters.

using two different inversion algorithms and using different methods of correction for the unknown local site gains, or 'static shifts'. The seismic data were reprocessed using a sequence that maintained amplitude information as close as possible to that giving a constant dependence on the magnitudes of the impedance contrasts. The depths to a mid-crustal zone of increased conductivity and sharp increase in reflectivity amplitude are correlated with temperatures from geothermal models of the region. We then draw inferences about the cause of these spatially correlating features and about the state of the middle and lower crust in this region.

LITHOPROBE SOUTHERN CORDILLERA MT SURVEY

Previous magnetotelluric results

That much of the lower crust and/or uppermost mantle of the Canadian Cordillera displays anomalously high electrical conductivity has been known for three decades (Caner & Cannon 1965; Caner *et al.* 1969). Caner (1970) interpreted this as evidence in south-western British Columbia for either (a) an upwelling of the mantle isotherm to produce partial melting in the lower crust, or (b) a hydrated lower crust, as suggested by Hyndman & Hyndman (1968) as a generic cause for enhanced conductivity in the lower crust. By 'hydrated' Caner meant 'wet', not a zone of hydrated minerals such as serpentine. It is important to note that, contrary to the initial conclusions of Stesky & Brace (1978), hydrated minerals do not *per se* have high conductivity; it is the fluids released during the dehydration reactions that cause the observed conductivity increase (Olhoeft 1981).

A large-scale geomagnetic depth sounding (GDS) magnetometer array study in 1980 (Gough *et al.* 1982) confirmed both the validity of approximating the gross regional structure by a 2-D model and the existence of a zone of anomalously high conductivity beneath much of the Canadian cordillera, named the Canadian Cordilleran Regional (CCR) conductor by Gough (1986a). A large GDS array in the north-western US states, operated as part of the EMSLAB project (EMSLAB 1988; Booker & Chave 1989), mapped the continuation of the CCR conductor into the state of Washington, where it appears to be bounded on its western edge by resistive blocks associated with the Columbia Embayment and the Blue Mountains (Gough *et al.* 1989). In this latter paper it was concluded that the CCR is indeed at lower crustal depths.

More recently, MT surveys that complement the LITHOPROBE ones were conducted to the north of our study area by Ian Gough and his colleagues (Majorowicz & Gough 1991; Gough & Majorowicz 1992). The period range of Gough's MT instrumentation is smaller than that of the LITHOPROBE survey, 130 Hz–62.5 s compared to 384 Hz–1820 s, and therefore provides less information on both the uppermost crust and on the lower crust and upper mantle. Those authors have interpreted one-dimensionally the *effective* apparent resistivities and phases, which are computed from the effective impedances given by the square root of the determinant of the MT impedance tensor (Berdichevsky & Dmitriev 1976). The effective phases have the advantage that they are largely unaffected by galvanic

distortion; however, one must exercise caution when constructing these effective impedances as the determinant becomes unstable in the presence of either high noise levels or severe distortion, or both (see, e.g. Groom *et al.* 1993). The main conclusion of Majorowicz & Gough (1991) is that the middle crust is everywhere conductive, about 10 Ω m at depths of 10–15 km. They further suggested a correlation between the conductivity of the middle crust and heat flow; the high phases becoming shallower with increasing heat flow.

Jones *et al.* (1990, 1991, 1992) presented an initial interpretation of the new LITHOPROBE MT data from the whole of southern British Columbia and south-western Alberta, with emphasis on the broad regional pattern of conductivity structure in the southern Canadian Cordillera. To gain qualitative insight they considered the effective phases in pseudo-section form and showed that the regional phase variation correlates spatially, to first order, with the morphogeological belt boundaries. The main result of Jones *et al.* (1992a) of relevance here is the contrast between the 60°–65° phase values at 10 s observed throughout the Intermontane belt, compared to the higher values (>75°) for the Omineca belt. This phase difference implies at least half-an-order of magnitude higher conductivity for the middle and lower crust beneath the Omineca compared to beneath the Intermontane belt.

For quantitative analysis, Jones *et al.* (1992) corrected their data for static-shift effects by fitting the strike-parallel apparent resistivity curves (*E*-polarization mode, see below) at a period of 10 s to a low-order polynomial, based on the regional distribution of apparent resistivity values. This method was preferred because it gave the most stable image on a regional scale (Jones *et al.* 1992). However, it corresponds to restricting the lateral large-scale resistivity variation at mid-crustal depths, so that variations in the deep crustal resistivity are poorly resolved. The results presented in this article are focused on local lateral variations in the middle and lower crustal resistivity and depth, so different approaches to static-shift corrections are used.

MT data acquisition

As part of the multidisciplinary LITHOPROBE Southern Cordillera transect investigations, wide-band MT data were acquired in 1989 and 1990 at 160 locations across southern British Columbia through contracts to Phoenix Geophysics (Toronto) Ltd. The 1989 sites were approximately coincident with the multichannel seismic lines (Fig. 2) acquired a year earlier, whereas the 1990 sites were located on a parallel east–west transect some 100 km to the south with north–south strike profiles connecting the two (Fig. 2). At each MT station, measurements were made of all three components of the time-varying magnetic field and two horizontal components of the electric field. In addition, the two horizontal components of the magnetic field were simultaneously recorded at a location usually 2 km distant to facilitate remote-reference processing for bias-error removal (Gamble, Goubau & Clarke 1979). The magnetic field components were measured with high-sensitivity iron-cored induction coils, and the electric-field components with lead–lead chloride (Pb–PbCl) electrodes. Recording sessions lasted typically two days, but on occasion up to five days depending on signal strength, and data were recorded over six decades of frequency from 384 Hz to 1820 s. Data at high frequencies (frequencies above 10 Hz) were acquired and processed in narrow frequency bands with two estimates per band. At longer periods, below frequencies of 10 Hz,

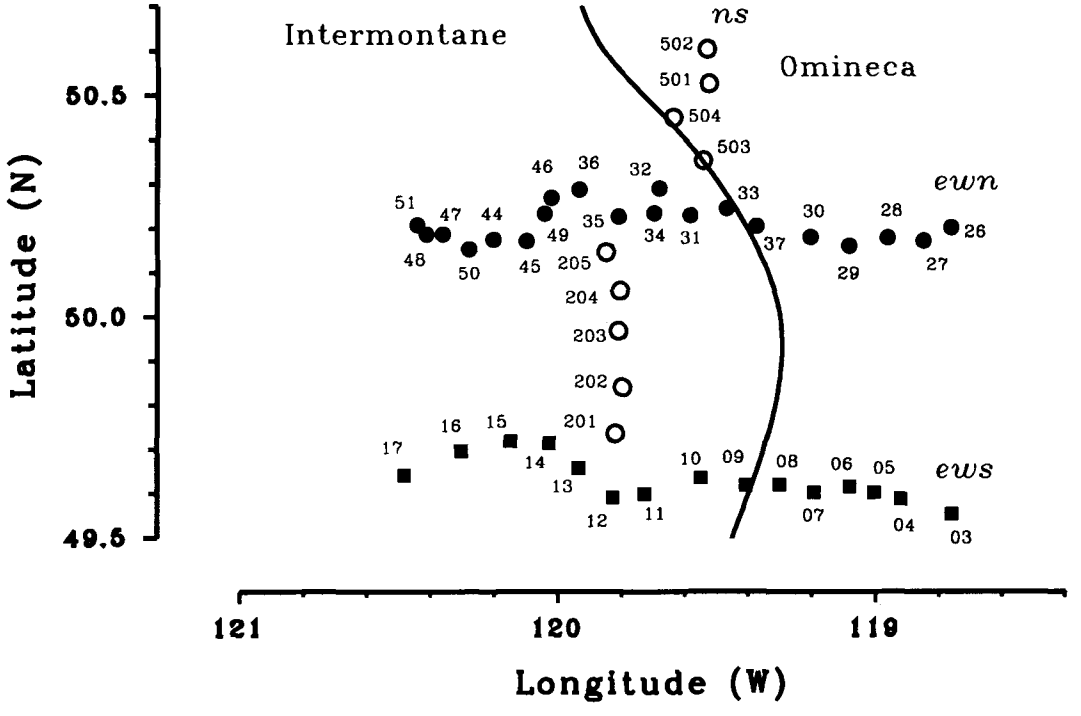

Figure 2. Locations of the magnetotelluric stations. Three profiles are discussed in this paper: two east–west profiles (*ews* and *ewn*), and one north–south profile (*ns*). The boundary between the Intermontane and Omineca belts is also shown.

cascade decimation acquisition and precessing were used (Wight, Bostick & Smith 1977). At all sites, recording continued until the averaged responses were of sufficiently high quality (better than a few per cent standard error), with a minimum of 40 hr of time series per site.

In this article, we discuss data from three profiles of MT stations; two are east–west profiles and are termed east–west north (*ewn*) and east–west south (*ews*), whereas the third is a connecting strike profile that we term north–south (*ns*) (Fig. 2). Profile *ewn* is collocated with the LITHOPROBE seismic-reflection data.

MT data processing: dimensionality and directionality indicators and distortion correction

We will not review the theory for processing and interpretation of MT data. Overviews of the methods to the early 1980s can be found in Kaufman & Keller (1981) and Vozoff (1986). General interpretation of MT data in terms of 3-D structures of all scale sizes is not yet possible. We do account for local, near-surface inhomogeneities, which cause principally electric field distortions, by assuming a model of the earth in which these distorting structures are treated as scatterers of galvanic current overlying a 1-D or 2-D regional earth. We used the matrix decomposition following Groom & Bailey (1989, 1991; see also Groom *et al.* 1993), extended for multiple frequencies and multiple sites (McNeice & Jones, private communication). The MT impedances for the mode in which current flows *parallel* to strike are termed the *E-polarization* data, whereas those for current flowing *perpendicular* to strike are the *B-polarization* data.

We subdivided the data set into overlapping frequency bands, each one decade in width. Within each band, the best-fitting frequency-independent telluric distortion parameters (characterized as *twist* and *shear*) and regional 2-D strike were determined. In addition, for specific site subsets, the most subset-consistent strike in each band was sought. Fig. 3 illustrates the strike directions from each site for five decades; (a) 100–10 Hz, (b) 10–1 Hz, (c) 1–10 s, (d) 10–100 s, and (e) 100–1000 s. The length of each arrow is a measure of the fit of the data to the assumed distortion model; long arrows (e.g. most arrows in Fig. 3e) indicate that the data fit the distortion model to within statistical tolerances ($\chi^2 < 4$), whereas short arrows indicate that the distortion model is an inadequate description of the effects; this can imply that either 3-D induction from large-scale features is present in the data or that the error estimates are too small.

Apparent in Fig. 3 is that there is 3-D distortion in the vicinity of the junction of the *ns* and *ewn* lines. In comparison, the data from all sites on the *ews* line fit the distortion model well and show a remarkably consistent strike direction. However, this direction depends on frequency, displaying a clockwise rotation with increasing period. Fig. 4 displays the best-fitting strike direction as a function of increasing period, i.e. increasing depth penetration, for the *ews* line. At frequencies greater than 10 Hz, corresponding to penetration depths of 5–10 km into the crust, the geoelectric strike is N25°W. At lower frequencies (longer periods) where the fields are sampling the middle and lower crust, the strike rotates clockwise to N20°E. At even longer periods, over 100 s, where the fields are sampling the uppermost mantle, this rotation increases to a strike of around N60°E. Thus, whereas the strike for the upper crust corresponds with the general geological strike of the region, the bulk of the crust has a different geoelectric strike which is not apparent in the surface geology. This observation is consistent with a model of tectonic assemblage for the Cordillera of surface terranes, some 5–10 km thick, thrust on top of the bulk of the crust. The variability in strike directions indicate the 3-D complexity of the crust in the region. The mantle strike will not be discussed further in this paper. The reader is referred to Jones, Groom & Kurtz (1993) for a discussion of this observation from interpretation of MT data acquired across the Kootenay Arc to the east.

The depth-dependent geoelectric strike data do not support any of the three geometric interpretations of the seismic data across the Okanagan Lake by Cook *et al.* (1992, their Fig. 8; their preferred interpretation is shown later in our Fig. 17) of a very thin cover of accreted rocks to the east of the lake (<3 km) compared to a very thick sequence (>20 km) to the west. If that were true, then the strike directions at periods sampling the mid-crust (10 Hz to 10 s, Figs 3b and 3c) should show a difference on either side of the lake, with those stations to the west giving a strike of N25°W and those to the east giving a different strike, in this case N20°E. Note that the figures show some differences in strike between the two east–west profiles, which suggests along-strike variability. This is discussed further in the comparison of the geoelectric models below.

This depth-dependent strike emphasizes Jones & Groom's (1993) position that geoelectric strike at a particular period cannot be assumed to correspond to local geological surface strike. The strike direction must be determined from the data themselves. In this case, a strike based on surface geology would be in error by 40°–50° for the bulk of the crust, and certainly for the region of the crust of interest in this paper.

Since this paper focuses on the middle and lower crust, a strike direction of N20°E was adopted for all frequencies and all sites. The data were not rotated into that direction, rather a seven-parameter distortion model, with one parameter (*strike*) fixed and two parameters (*twist* and *shear*) frequency invariant, was fit to the data (see Jones & Groom 1993). The anisotropy, or curve splitting, at each site was corrected by shifting the *E*-polarization mode and *B*-polarization-mode ρ_a data to their geometric mean at the high frequencies (frequencies higher than 30 Hz).

Site-gain correction

Having fit a distortion model that removed the phase mixing caused by galvanic scattering and corrected for local site anisotropy, what remains is a single parameter at each site named by Groom & Bailey (1989) the *site gain, g*. This site gain corresponds to the static-shift effect seen on MT data. The apparent resistivity (ρ_a) data are multiplied by a frequency-independent constant such that the ρ_a curves, when plotted on a logarithmic ordinate, are shifted up or down whereas the phase (ϕ) data are unaffected (e.g. Jones 1988; Sternberg, Washburne & Pellerin 1988; Jiracek 1990). The *E*- and *B*-polarization-mode data from all sites are

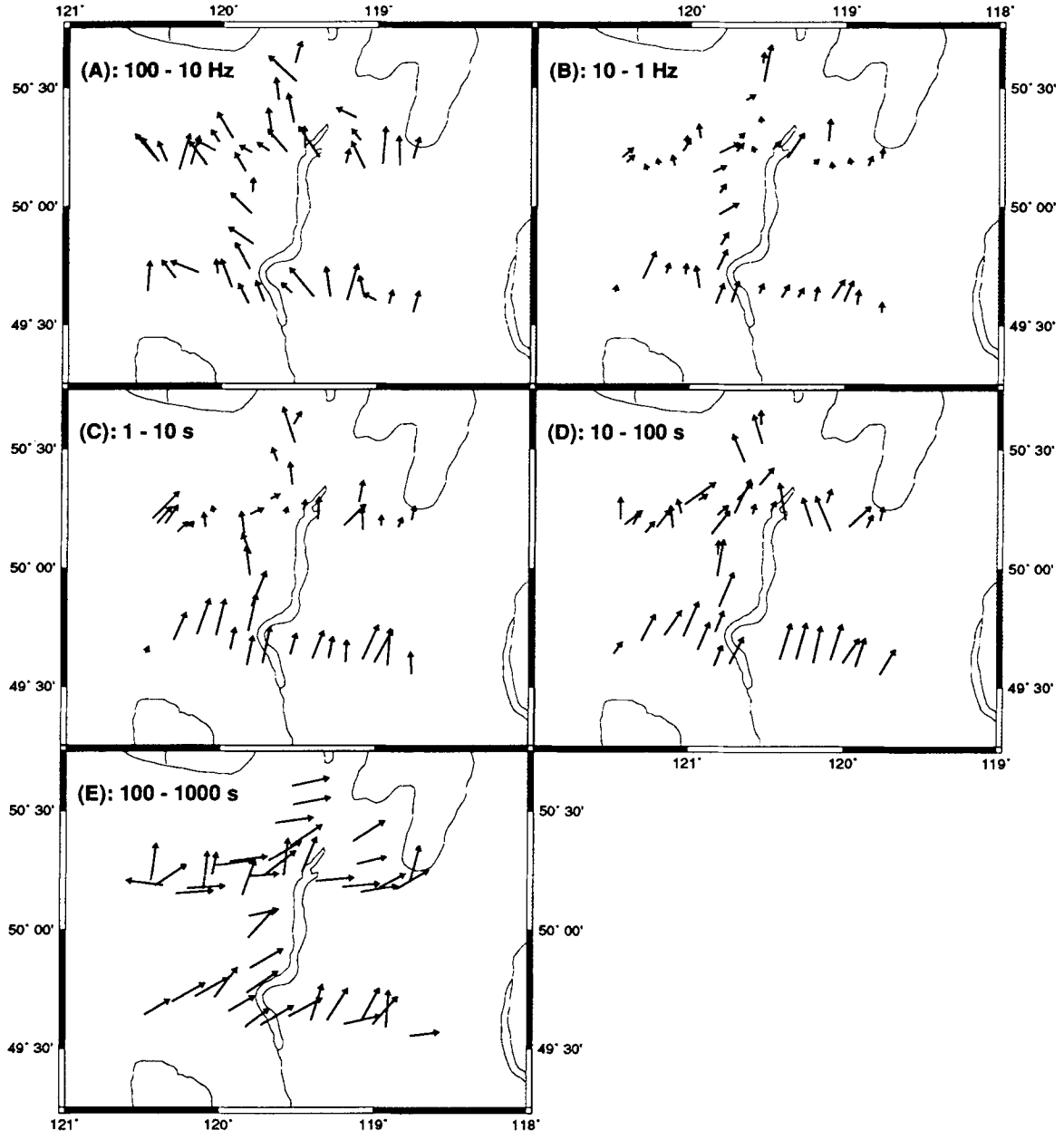

Figure 3. Strike directions derived in five periods bands; (a) 100–10 Hz, (b) 10–1 Hz, (c) 1–10 s, (d) 10–100 s, (e) 100–1000 s. The length of each arrow is a measure of the fit to a Groom–Bailey distortion model; long arrows fit well, short ones fit badly. The MT stations are located at the base of the arrows.

illustrated in Figs 5, 6 and 7 (locations in Fig. 2). The similarity of the ϕ plots is in stark contrast to the spread of the ρ_a curves, which generally have the same shape but are displaced from one another. In addition, the E- and B-polarization-mode phases at most stations have similar values at long periods, which indicates that this deep resistivity is close to 1-D, i.e. the deeper part of the section is close to horizontally layered. In this paper we have applied two types of methods for correcting the unknown site gains. One of the types of methods is applied to the data themselves, whereas the other type is applied to the model, either in the form of a model parameter or as part of the inversion procedure.

The simplest approach for data correction is to assume that the earth below a given depth is 1-D, which requires the E-polarization-mode ρ_a curves to have the same long-period asymptote (e.g. Berdichevsky, Vanyan & Dmitriev 1989). The phase curves being approximately coincident at long periods implies that the true static-shift corrected apparent resistivity curves for the E-polarization mode should also be nearly coincident at those periods. A somewhat less restrictive assumption is to require the long-period data to follow a simple regional trend (Jones *et al.* 1992). A problem with such a parametric approach is data that are consistently biased over a large region. A regional bias is, in fact, apparent in our data as illustrated in Fig. 8 that shows 3-D contour plots of the E-polarization-mode resistivities and phases at 227 s from all the sites. Whereas the phase

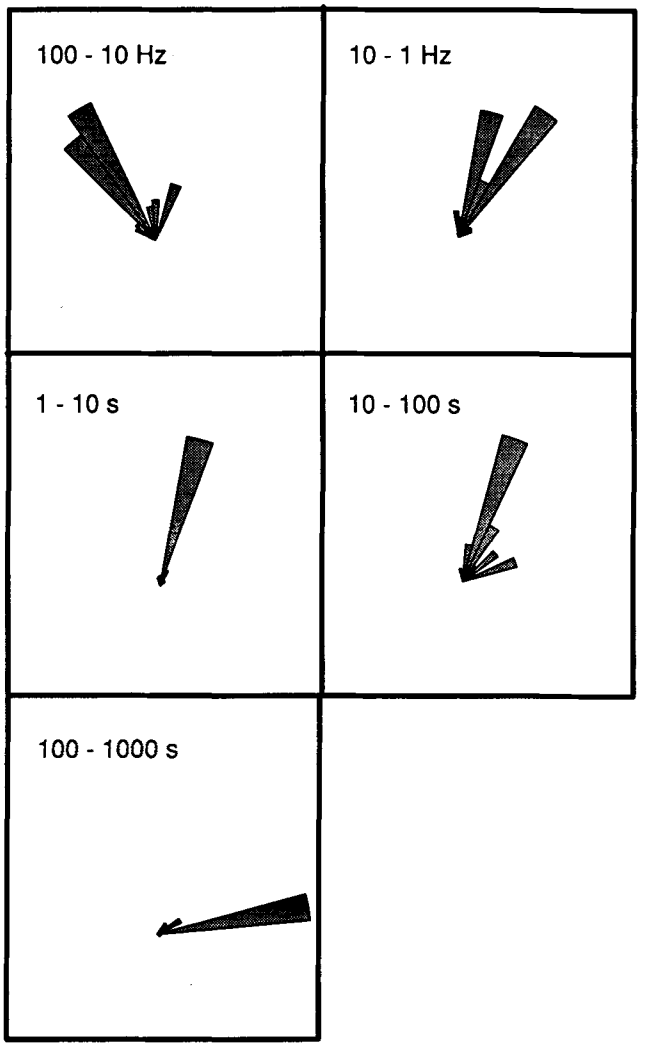

Figure 4. Weighted strike rose histograms the five period bands in Fig. 3 from all sites on the *ews* line. The weights used were based on the inverse measure of misfit to the distortion model.

map indicates a regional SE–NW increase in phase by about 8°, the resistivity map infers a regional decrease in resistivity from SW–NE by two orders of magnitude. This apparent inconsistency is explained by the presence of a highly resistive mid-Jurassic granitic intrusion (e.g. the Osprey Lakes batholith) in the south-west. Thus, the ρ_a data from sites 113–117 are all biased upwards compared to their correct regional value. For this study, the *E*-polarization mode ρ_a data were first fit to a cubic spline (to compensate for some of the sites having incomplete period coverage) and the ρ_a curve was shifted such that the value at the longest period sampled, 1820 s, was 50 Ω m. This period corresponds to a penetration depth of 50 km or more, i.e. well into the mantle at all sites. This ρ_a value is representative of the behaviour of a majority of stations at this periods, excluding the few with extreme values. The same correcting factor was applied to the *B*-polarization-mode ρ_a data.

In the model-based approach that we have used, site gains were determined as part of the inversion procedure requiring the smoothest model that fits the observations (deGroot-Hedlin 1991). However, rather than permit the static-shift factors from all sites to vary, and differing factors for the *E*- and *B*-polarization data at each site, we utilized Smith & Booker's (1991) rapid relaxation inversion (RRI) algorithm and designated certain sites (see below) as having the correct level whilst simultaneously requiring that the same shift factor be used for both the *E*- and *B*-polarization-mode data at each site.

Phase pseudo-sections

Pseudo-sections of the *E*- and *B*-polarization-mode phases from the two east–west profiles are shown in Figs 9 (*ewn*) and 10 (*ews*). The vertical scale of logarithm (base 10) of period is a non-linear function of depth, the equivalent depths depending on the resistivity-depth variation. There is local variability in the short-period phases indicating near-surface variations in resistivity, but the long-period phases are high (>50°) across the whole profile. This is a reliable indication of the presence of a low-resistivity layer at middle to lower crustal depths, since phase curves are not affected by static shift. Note that the 50° phase level is shallower in the eastern part of the section (Omineca belt) than in the western and central parts (Intermontane belt). This is a reliable indication that the conductive deep crust is either shallower or more conductive beneath the Omineca compared to the Intermontane belt.

2-D inversions

After the above processing, the data were modelled using two different inversion algorithms. In both routines, *E*- and *B*-polarization modes were modelled simultaneously. Inversion of only *E*-polarization-mode data resolves well only the depth and the conductivity-thickness product of the conducting regions, whereas inversion of only *B*-polarization-mode data resolves well their horizontal extent and the presence of thin resistive layers (Agarwal, Poll & Weaver 1993). Using both modes in the inversion allows for a much better evaluation of the resistivity structure over a large area. A comparison of the results from the two different algorithms gives insight into model-parameter resolution. Agarwal, Poll & Weaver's (1993) code seeks the simplest model in terms of the least number of bodies of different, but constant, resistivity, whereas Smith & Booker's (1991) seeks the smoothest model, in terms of least variation of conductivity both laterally and vertically, which fits the data.

(a) Agarwal, Poll & Weaver's algorithm

The MT data were site-gain corrected using the asymptotic limit, as described above, and were inverted to resistivity-depth profiles in two steps. First the *E*-polarization-mode data at each station were inverted individually to obtain a series of adjacent 1-D resistivity-depth profiles using Weaver & Agarwal's (1992) procedure. The second step was a 2-D inversion of the multistation data using the technique of Agarwal, Poll & Weaver (1993; hereafter referred to as APW), which is based on an iterative scheme for minimizing the misfit of 2-D forward models (forward method described

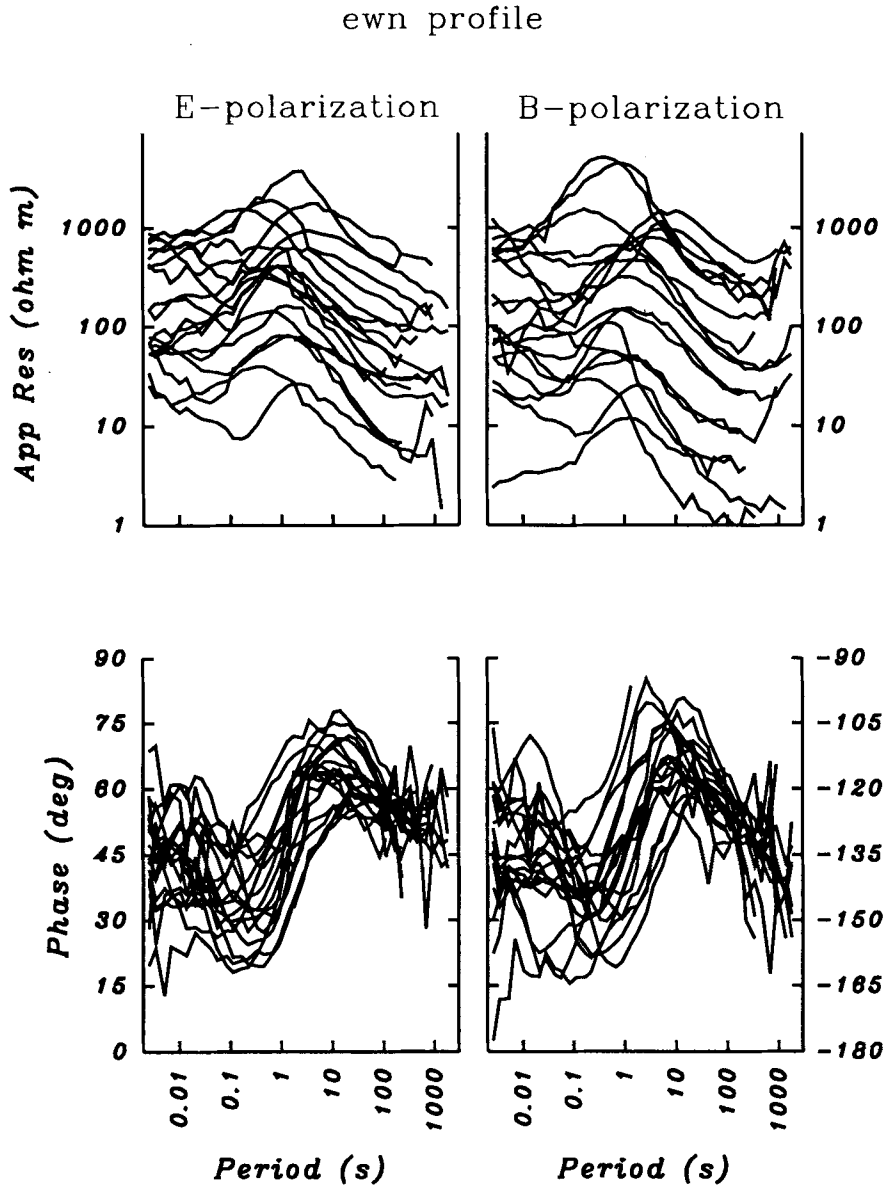

Figure 5. MT data corrected by the Groom–Bailey procedure from all sites from the *ewn* profile. Top: apparent resistivity; bottom: phase; left: *E*-polarization-mode data; right: *B*-polarization-mode data.

in Poll, Weaver & Jones 1989), with the 1-D models stitched together as the starting model.

East–west north profile. The apparent resistivity curves corrected for static shift are shown in Fig. 11. The phase curves, which are not corrected, are not shown again (see bottom of Fig. 5). However the near-surface two-dimensionality remains; there is still over an order of magnitude scatter at short periods indicating that the near-surface resistivity indeed varies significantly. At intermediate (10–100 s) and longer (>100 s) periods, the *E*-polarization-mode ρ_a curves show little variation (half an order of magnitude), indicating that the deep crust has a reasonably consistent value of resistivity along strike.

1-D inversions of the gain-corrected *E*-polarization-mode data are shown at the top of Fig. 12. It can be seen that the near-surface resistivity values exhibit large scatter, probably mainly dependent upon whether the stations are on conductive sedimentary cover or resistive igneous plutons. The most important feature for our study is the decrease in resistivity at mid-to-lower crustal depths (15 to 28 km at the top of the low-resistivity layer) for all stations. This is in agreement with what has been observed in most MT surveys in Phanerozoic terrains (e.g. Haak & Hutton 1986; Hyndman & Shearer 1989). The resistivity in these layers ranges from 30 to 60 Ω m, similar to the 'Canadian Cordilleran Regional Conductor' (Caner 1971; Gough 1986b) and the 'Mainland Conductor' reported in Kurtz, DeLaurier & Gupta (1990).

The APW 2-D inversion procedure is computer intensive. We followed their approach to seek the model that best fits the data and simultaneously has the smallest number of resistivity blocks. To reduce the required computational effort further, we only used data at periods between 1.3 and 455 s, the period range influenced by the deep crustal structure. The minimum-misfit model (3.1 per cent after 539

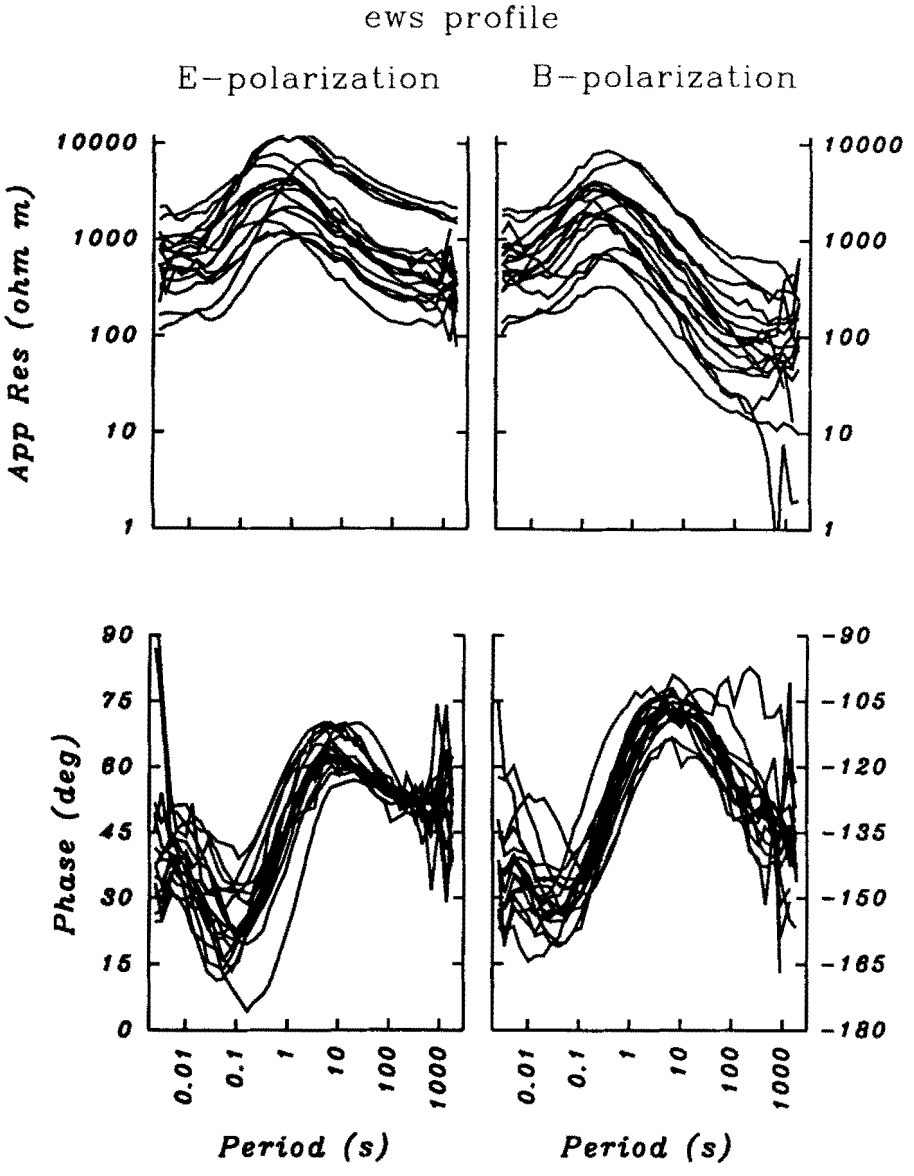

Figure 6. Same as Fig. 5 for the *ews* profile.

iterations) obtained for the *ewn* profile is shown at the bottom of Fig. 12: its resistivity structure is much simpler than using the 1-D results. The mid-crustal conductive layer is well defined: its top is at 17 km depth in the west and 10 km in the east of the Intermontane Belt part of our study area, and 8 km depth for the western part of the Omineca Belt. The actual deep crustal resistivity is half an order of magnitude higher under the Intermontane Belt than under the Omineca Belt.

East–west south profile. A composite plot of 1-D inversions from the site corrected *E*-polarization-mode data (Fig. 11b) from the *ews* profile is shown in Fig. 13 (top). The final 2-D model (Fig. 13, bottom; misfit 2.8 per cent after 236 iterations) is very simple and its features are similar to the *ewn* model: here also the mid-crustal conductor gets shallower from the Intermontane to the Omineca Belt (from 20 to 17 km under the Intermontane and 13 km under the Omineca) and the resistivity values are also the same. The layer is, however, everywhere deeper than in the *ewn* model. The misfit of the final *ews* model is about half that of the final *ewn* model, indicating that the *ews* profile resistivity structure is closer to a 2-D model than the *ewn* profile, as shown by their larger strike arrows on Figs 3(c), (d) and (e).

North–south profile. Data from the *ns* profile have also been corrected (Fig. 11c) and inverted. The progression in depth to the conductor mentioned above is also present in the best-fitting 2-D *ns* model (Fig. 14; misfit 3.6 per cent after 471 iterations). The observation made above and implied by the strike information is confirmed: the depth to the conductor decreases from south to north, corresponding to an increase in inferred lower crustal temperatures to the north-east (Lewis, Bentkowski & Hyndman 1992).

(b) Smith & Booker's algorithm

Simultaneous inversions of both *E*- and *B*-polarization-mode data from the two profiles *ewn* and *ews* were undertaken using Smith & Booker's (1991) rapid-relaxation inversion (RRI). Site gains were determined as part of the

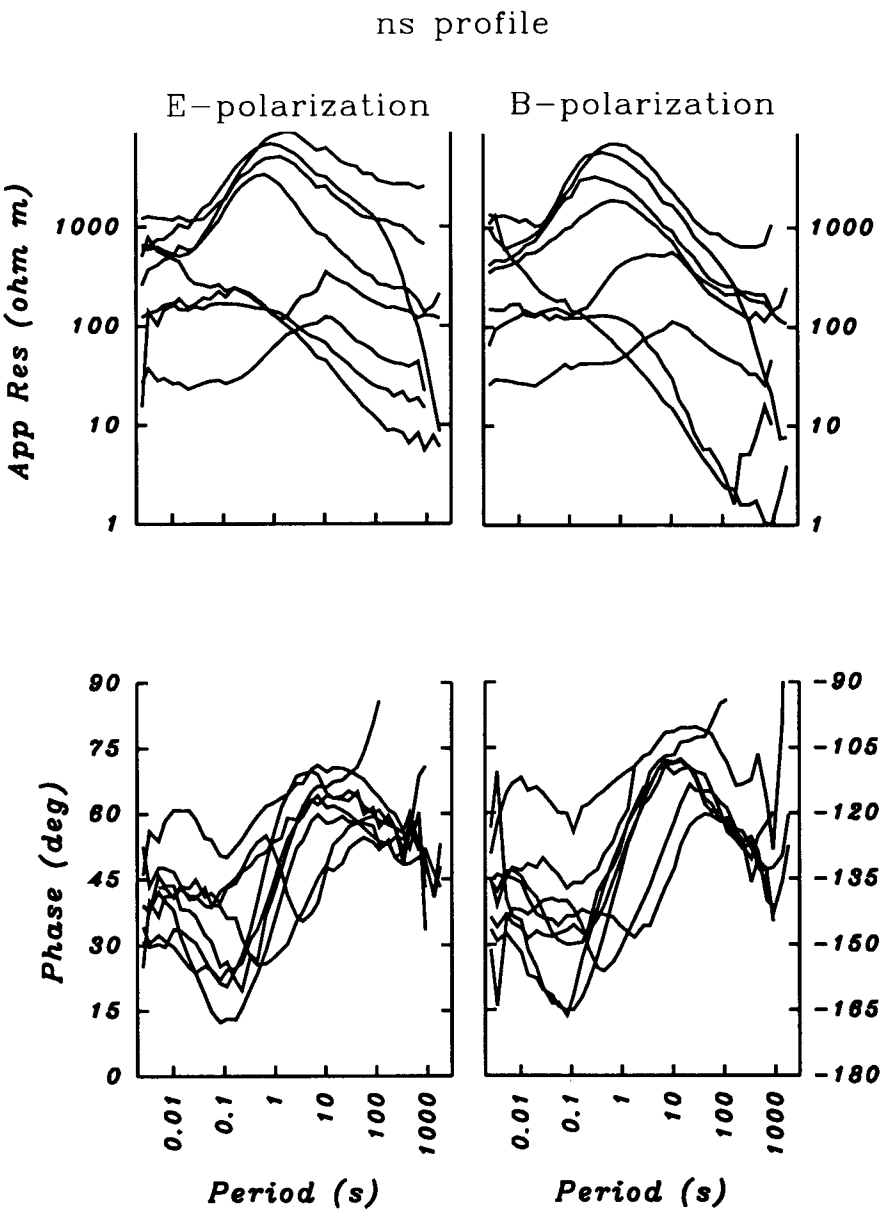

Figure 7. Same as Fig. 5 for the *ns* profile.

procedure. However, it is necessary to constrain at least one resistivity curve, thus some assumption must be made about the regional levels, or the algorithm puts all structural variation into the site gains. The *E*-polarization-mode phases (Figs 9 and 10) indicate that there is a regional variation in crustal resistivity, and the averaged *E*-polarization mode resistivity at 100 s for the MT sites located on the Intermontane Belt is 200 Ω m, whereas for those sites located on the Omineca Belt is 80 Ω m. We have performed inversions of the data from both modes at 11 frequencies in the range 10 Hz–100 s from all 15 sites on the *ews* profile and all 20 sites on the *ewn* profile with the following constraints:

(a) the *E*- and *B*-polarization-mode resistivity curves for the middle site (site 037 for *ewn* and site 110 for *ews*) were shifted such that the *E*-polarization mode curves had values of 100 Ω m at 100 s. This value represents approximately the median value of all the available data. These curves were then held fixed in the inversions, whereas the curves at all other sites were permitted to vary their level (but with *E*- and *B*-polarization-mode ρ_a curves remaining together).

(b) The *E*- and *B*-polarization-mode resistivity curves for the three end sites of each profile were shifted such that their *E*-polarization-mode curves had a value of 200 Ω m in the Intermontane Belt and 80 Ω m in the Omineca Belt, at 100 s. These values represent approximately the medians of the sites within the respective belts. As above, these curves were held fixed in the inversions whereas the levels of the others were permitted to vary.

The resulting models from the above constraints are shown in Figs 15 and 16. To facilitate comparison with the models obtained using the APW code, there are only five contours with a contour interval of 0.5, so that the shading pattern is the same in all models. The models are plotted on a 1:1 scale, with a total depth extent of 30 km, and the

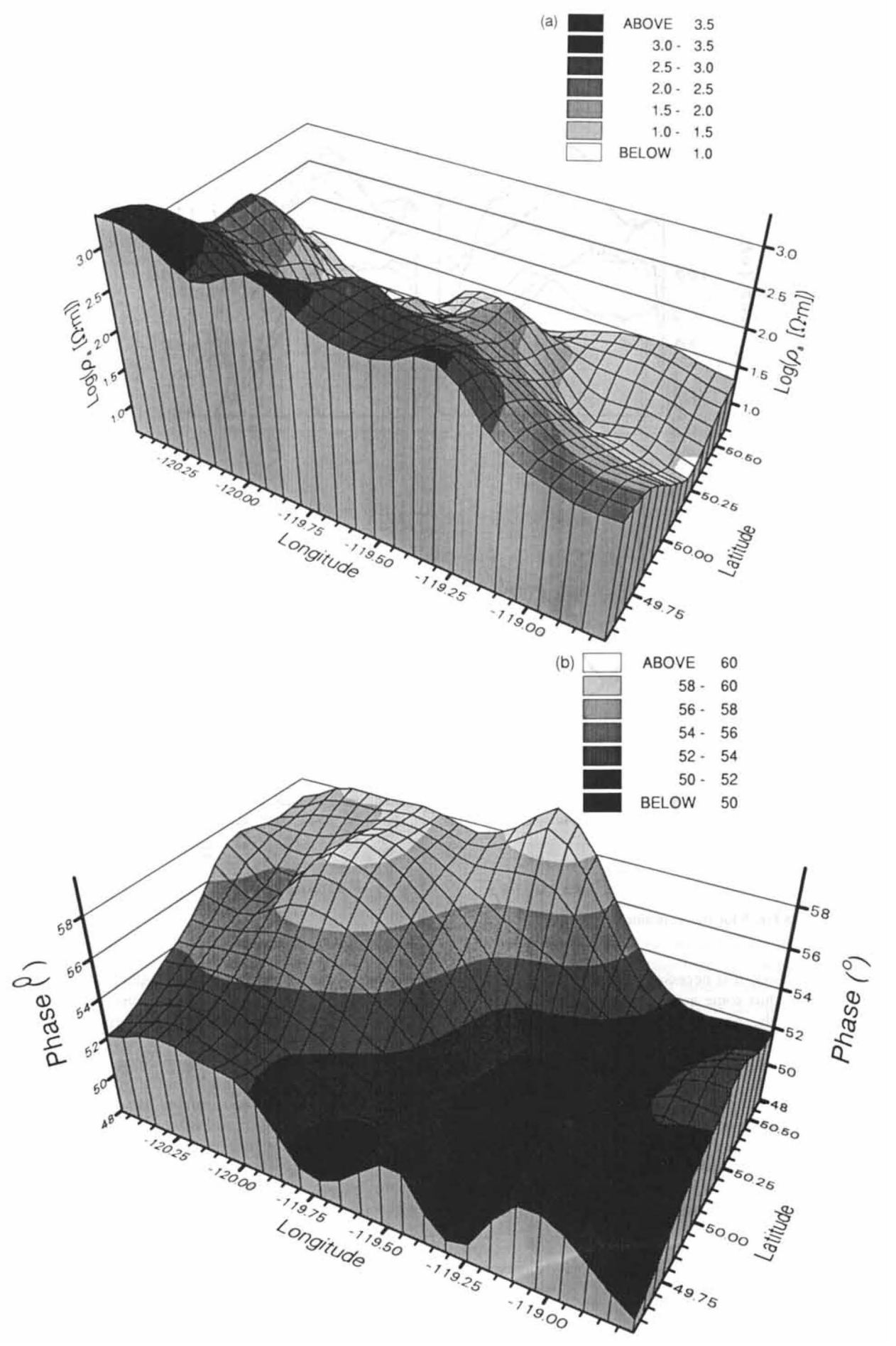

Figure 8. Perspective contour plots of the *E*-polarization-mode apparent resistivities (a) and phases (b) for all data, after removal of distortion effects, at a period of 227 s. Note the differing viewing angles for the two plots.

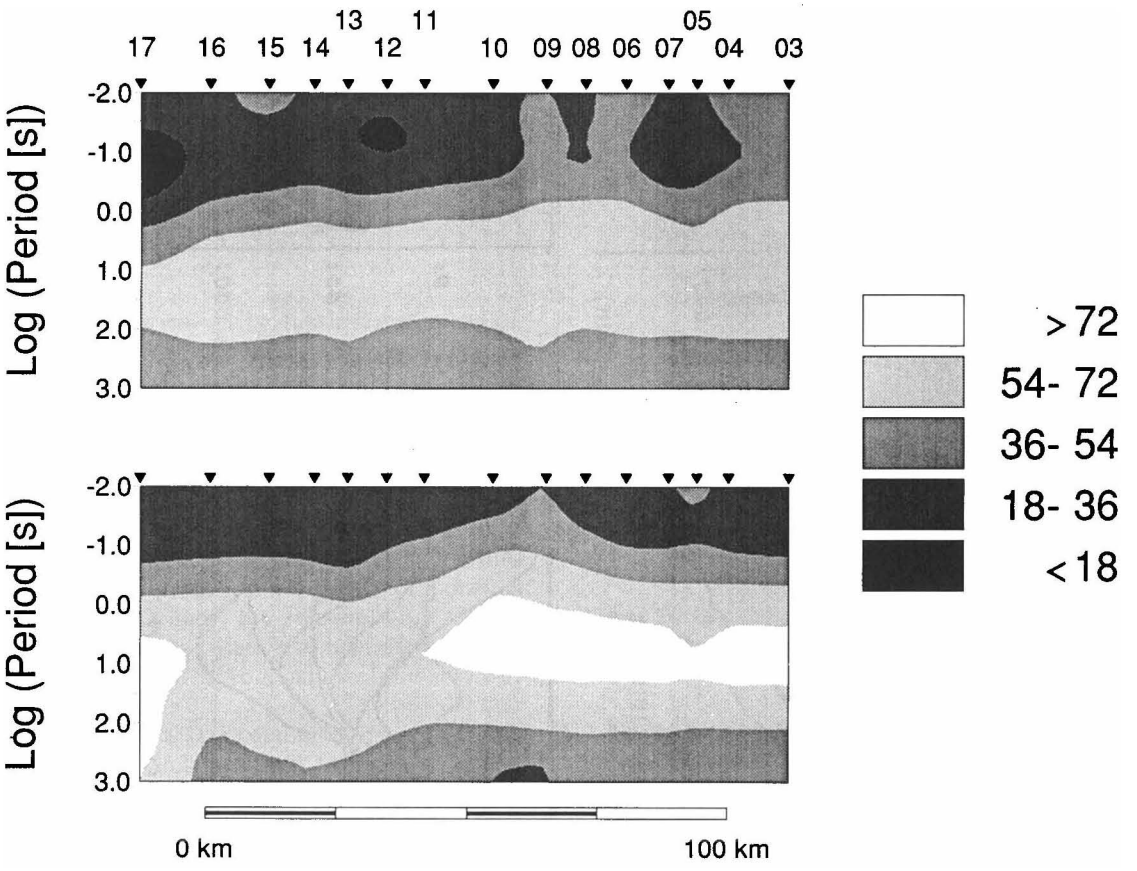

Figure 9. *E*- and *B*-polarization-mode phase pseudo-sections for the *ewn* line. The high phases observed at periods longer than 10 s are indicating a low-resistivity layer at mid to lower crustal depths.

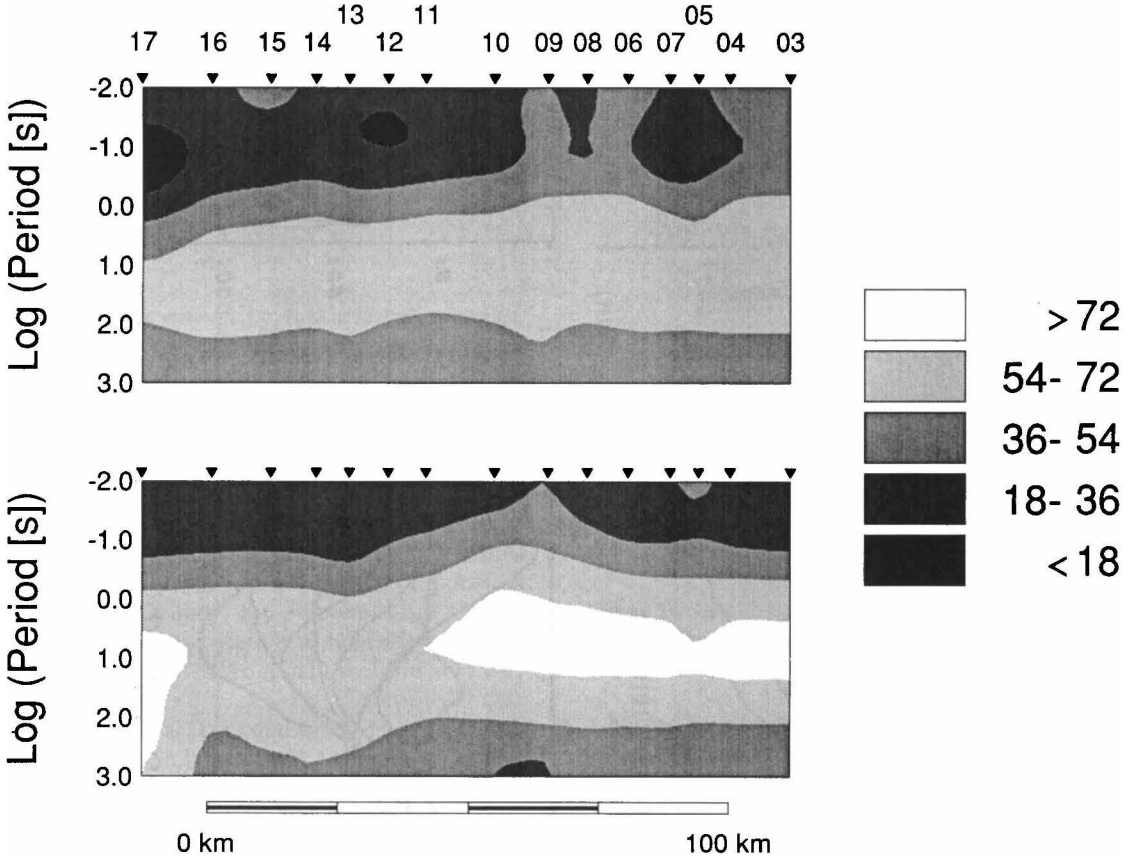

Figure 10. *E*- and *B*-polarization-mode phase pseudo-sections for the *ews* line.

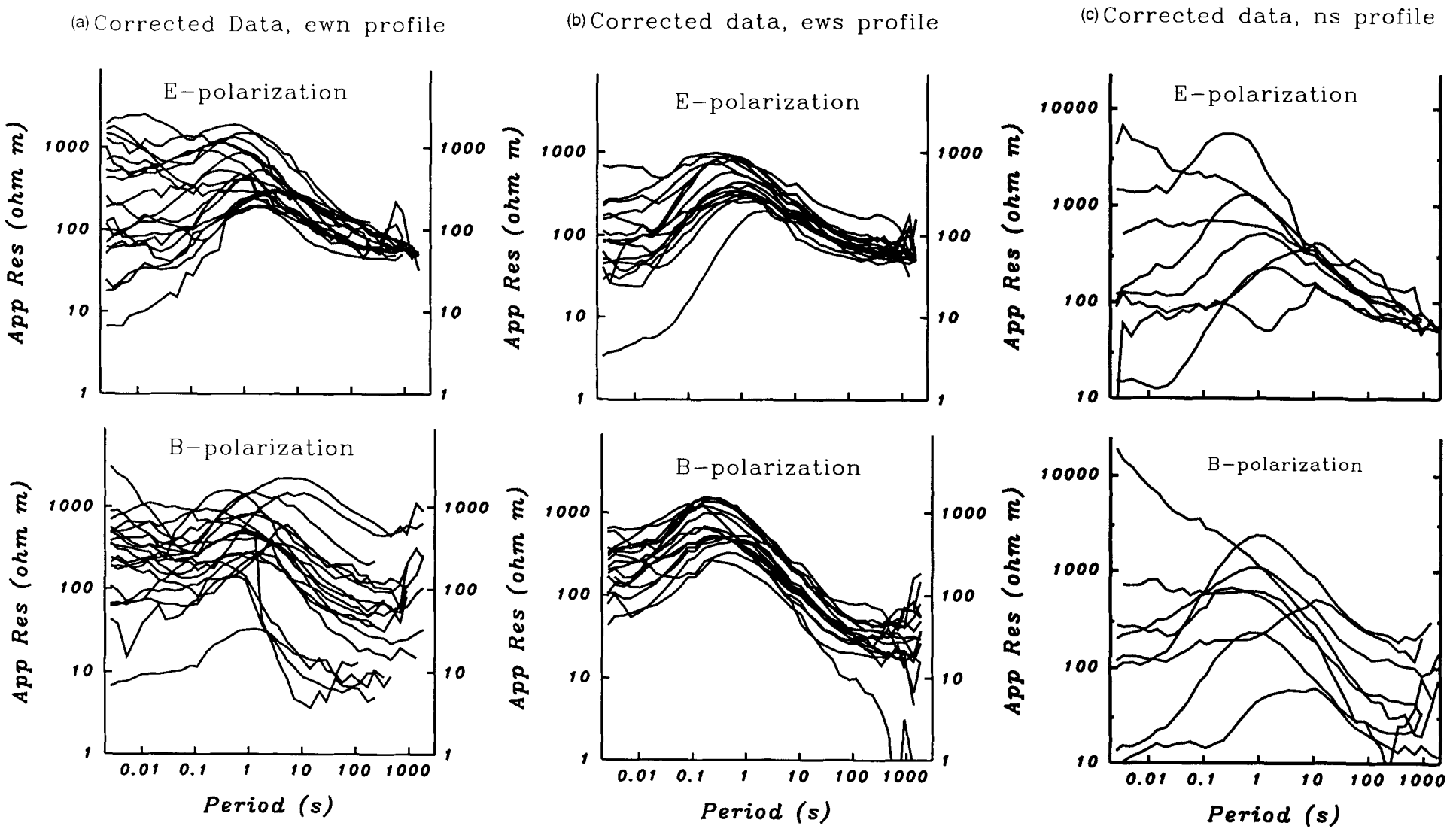

Figure 11. (a) *ewn*, (b) *ews*, and (c) *ns* profile apparent resistivity data with site-gain corrections applied by the long-period asymptote method (see text).

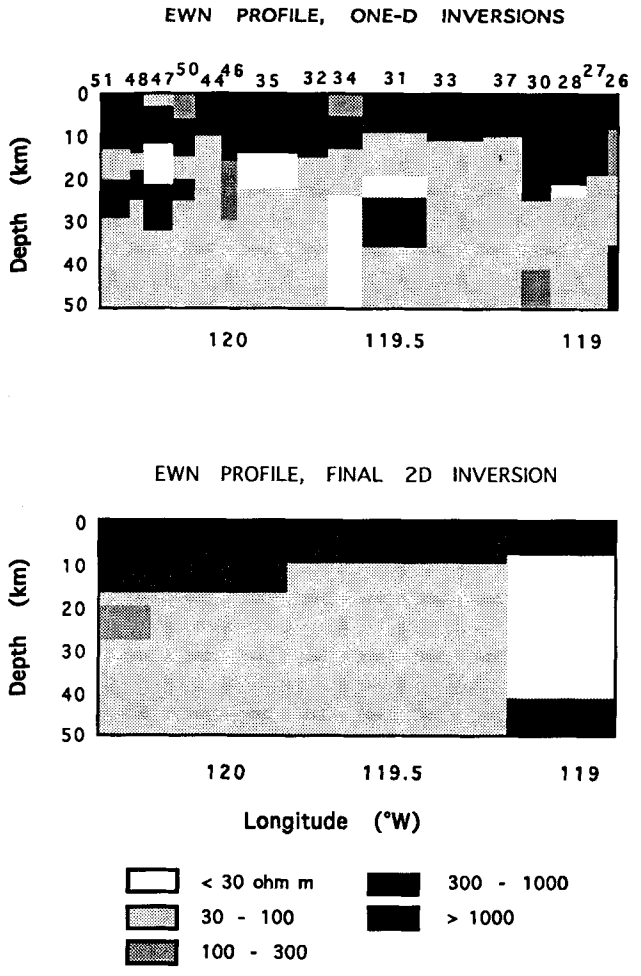

Figure 12. (a) 1-D inversion of corrected *E*-polarization-mode data, *ewn* profile. Note the general decrease in resistivity below 10 to 20 km depths. (b) Best-fitting model obtained from the 2-D inversion method of Agarwal, Poll & Weaver (APW) for the *ewn* profile data. Note the simplicity of the resistivity structure. The conducting layer gets shallower and more conductive from the Intermontane to the Omineca Belt.

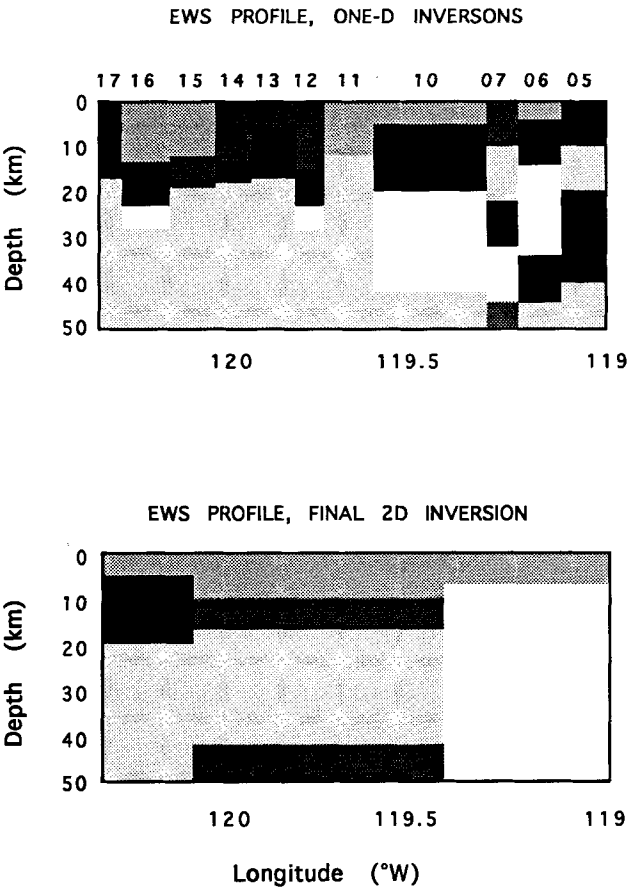

Figure 13. (a) 1-D inversion of corrected *E*-polarization-mode data, *ews* profile. (b) Best 2-D model for the *ews* profile, using the APW method. Again the conducting layer is shallower and more conductive under the Omineca Belt than under the Intermontane Belt, and is everywhere deeper than under the *ewn* profile.

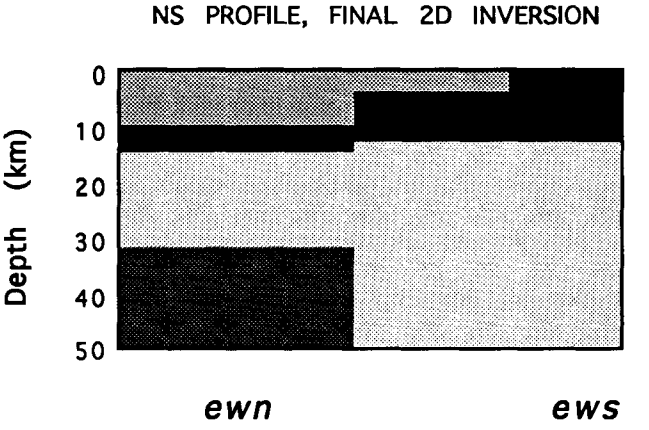

Figure 14. Best 2-D model, *ns* profile. It confirms the shallower depth to the conducting layer from the *ews* to the *ewn* profile.

locations of the sites are shown by the inverted triangles. The models of the *ewn* profile fit the phase data to within a 4.5° (upper model) and 2.5° (lower model) on average, whereas the *ews* data are fit to 5° and 3.5° on average (with equivalent misfit levels for ρ_a data).

The following features are evident.

(i) The models from the two profiles are similar in most features. This indicates that although the data from the sites in the middle of the *ewn* profile show evidence of induction due to a large-scale 3-D body, the responses can still be inverted in a 2-D manner and yield a comparable model of the subsurface to one obtained from data that are very 2-D (profile *ews*).

(ii) The depth to the 300 Ω m contour is greater beneath the Intermontane Belt than beneath the Omineca Belt. This is in accord with the above model study using the APW method and a different philosophy for correcting site gains.

(iii) The middle and lower crust beneath the Omineca belt is conducting, with a resistivity less than 30 Ω m, whereas beneath the Intermontane belt it is at least half an order of magnitude more resistive (100–300 Ω m). This is in accord with the image obtained by simple Niblett–Bostick transformation of the *E*-polarization-mode data, after site-gain correction by regional smoothing, in Jones *et al.* (1992), as well as with results shown in Figs 12 and 13.

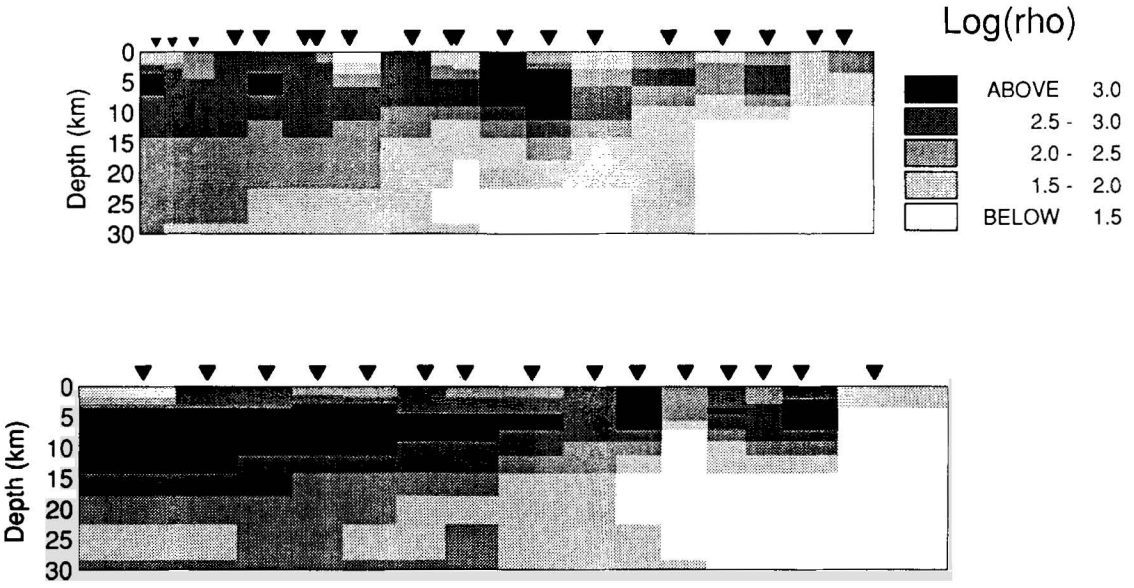

Figure 15. RRI models for the *ewn* (top) and *ews* (bottom) *E*- and *B*-polarization-mode data with the constraint that the ρ_a curves for the middle sites of each profile were held fixed after shifting such that the *E*-polarization-mode ρ_a value was 100 Ω m at 100 s. The ρ_a curves for all other sites were permitted to vary, but the *E*- and *B*-polarization-mode ρ_a data for each site were fixed relative to each other.

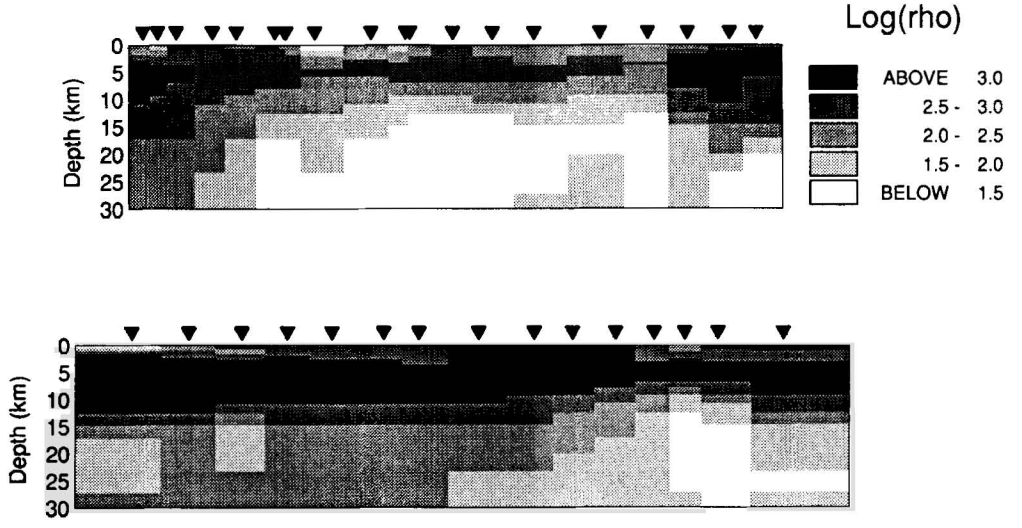

Figure 16. RRI models for the *ewn* (top) and *ews* (bottom) *E*- and *B*-polarization-mode data with the constraint that the ρ_a curves for the end three sites of each profile were held fixed after shifting such that the *E*-polarization-mode ρ_a value was 200 Ω m for the western end sites (Intermontane belt) and 80 Ω m at the eastern end sites (Omineca belt) at 100 s. The ρ_a curves for all other sites were permitted to vary.

MULTICHANNEL SEISMIC PROCESSING AND INTERPRETATION

As part of the LITHOPROBE Southern Cordillera Transect, multichannel seismic-reflection data were acquired in 1988 by Sonix Inc. of Calgary, and initial processing was done by Western Geophysical Ltd, and Cook, Varsek & Clowes (1991) and Cook *et al.* (1992; Fig. 17) presented structural interpretations of these data. They conclude that the west-dipping events in the upper-to-middle crust at the east of line 10 are the Okanagan Valley Fault that listrically flattens and merges into the lower crustal reflecting bands at about 7.0 s. The small east-dipping events at the west end of line 10 are interpreted as the Quilchena Creek Fault that bounds the east side of the Nicola Horst (Cook *et al.* 1992). High reflectivity is common in the lower crust on some sections. They have interpreted the general lower crustal reflectors as continuations of the Foreland–Omineca Belts gently dipping to the west for the upper part ($7 < t < 9$ s two-way traveltime), and as underlying autochthonous North America for the lower part ($9 < t < 11$ s). While the geological correlations with the seismic images for the upper crust are generally clear for the upper crust, these correlations for the lower crust are not strong.

The original processing was designed to emphasize structural discontinuities through the use of automatic gain control (AGC) and migration and coherency techniques (Cook *et al.* 1992). The sections do not preserve true

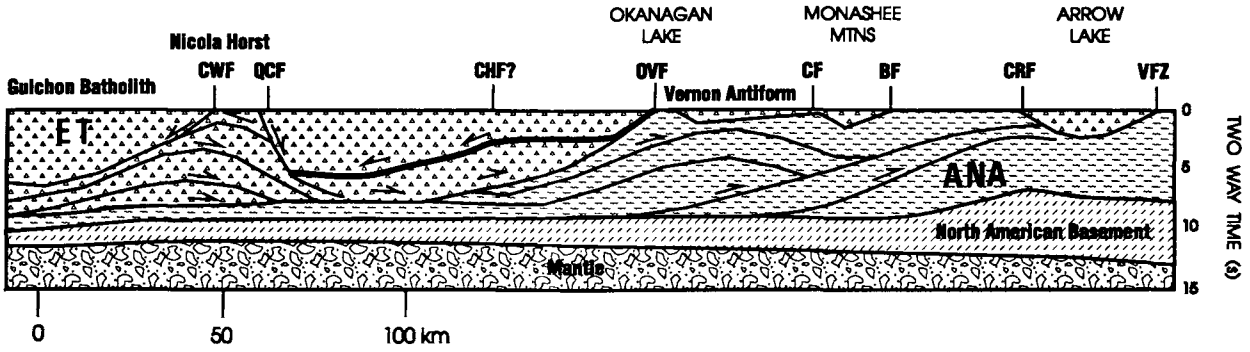

Figure 17. Interpretation of LITHOPROBE Line 10, from Cook *et al.* 1991. Faults: CWF: Coldwater, QCF: Quilchena Creek; CHF: Chapperon; OVF: Okanagan Valley; CF: Cherryville; BF: Beavan; CRF: Columbia River; VFZ: Valkyr. ET: Exotic terranes; ANA: Allochtonous North American rocks.

reflectivity amplitudes; AGC, while it may enhance small reflectors that would otherwise be missed, obliterates any information on the relative strengths of reflectors or reflection bands from different AGC windows. In order to study the true amplitude characteristics of the crust, the data were reprocessed.

This re-processing was performed at the LITHOPROBE Seismic Processing Facility in Calgary using the CYBER/DISCO system for pre-stack processing and the ITA/INSIGHT system for post-stack processing. Throughout the new processing sequence, the data were kept as close as possible to true relative amplitude. The starting data were true relative amplitude common-depth point (CDP) gathers of 18 s length. The data described as 'true relative amplitude' have been corrected for geometric spreading by a factor of $tV_{rms}(t)$, where t is the traveltime and $V_{rms}(t)$ is the root-mean-square velocity to traveltime t, which is suitable for a perfectly elastic medium. Functions of time only are more commonly used, but the velocity variations are not very large in this case, so the general appearance of the data would be quite similar to what will be shown here. The velocities used were determined by Western Geophysical Ltd as part of the original processing. After normal moveout corrections using the rms velocity values, each CDP gather was stacked into one trace. The traces were then truncated to 12.5 s, about one second below the Moho, and the first breaks and refracted arrivals were muted after stack to prevent them from dominating. There were no great differences in energy among the traces within CDP gathers, so whether the mutes were applied before or after stack made little difference. Trace balancing was necessary because of the large discrepancies in amplitude between stacked traces associated with vibrator and geophone ground coupling. After stack, all traces were energy-balanced over the whole 12.5 second range. This ensures that all traces have equal weight before further processing.

To reduce the effect of incoherent noise, a coherency/semblance filter (Milkereit & Spencer 1989) was applied to the whole section. We note that while the coherency filter improves the reflectivity definition, the pattern of higher reflectivity in the lower crust is evident in the section without this processing step. Coherency is calculated for many slowness, or dip, values (31 here) in a trace window (21 traces here), and the maximum coherency value is kept. Incoherent noise is greatly reduced. The number of dips used is quite small because the main focus is to emphasize flat-lying reflectors: there is thus a potential for the removal of coherent dipping events. However, comparison with sections processed for structural interpretation using a larger range of dips (see Cook *et al.* 1992) indicates that the main west-dipping events in the eastern part of the section were preserved. The number of traces used here requires coherency over distances of at least 400 m. The resulting section is shown in Fig. 18.

The reprocessed seismic section shows clearly that the lower crust is reflective on most lines. To obtain an objective evaluation of the evolution of the seismic reflectivity with depth, we have calculated energy histograms using the method of Bittner & Wever (1991; Fig. 19). It is clear that the overall reflectivity is strongly enhanced in the lower half of the crust and that the reflective layer becomes shallower from west to east. A detailed examination of the true relative amplitude section (Fig. 20) shows that while some of the lower crustal reflectors appear to dip gently, the dips are not systematic, some being to the east and some to the west. Many reflectors are flat over the distances resolved by the semblance filter (see Fig. 20). Therefore, while we cannot exclude the influence of structure, we conclude that many lower crustal reflectors are not primarily of structural origin; on this profile, and on other southern Cordilleran profiles, they appear to be continuous across terrane and structural boundaries. Certainly the top of the general enhanced lower crustal reflectivity is not appreciably offset by major upper crustal structural boundaries. Lewis *et al.* (1992) have pointed out an alternate interpretation that the reflectivity is not associated with structure but is a fundamental property of the Phanerozoic lower crust. They suggest a correlation between the depth of the lower crustal reflectivity and heat flow for the eastern part of the LITHOPROBE Southern Cordillera transect (Lines 2 to 5).

DEEP CRUSTAL TEMPERATURES

The third deep crustal parameter that appears to change across the Intermontane–Omineca boundary is temperature, as inferred from surface heat flow and radioactive heat-generation data. From previous studies, it has been suggested that globally the top of conductive and reflective

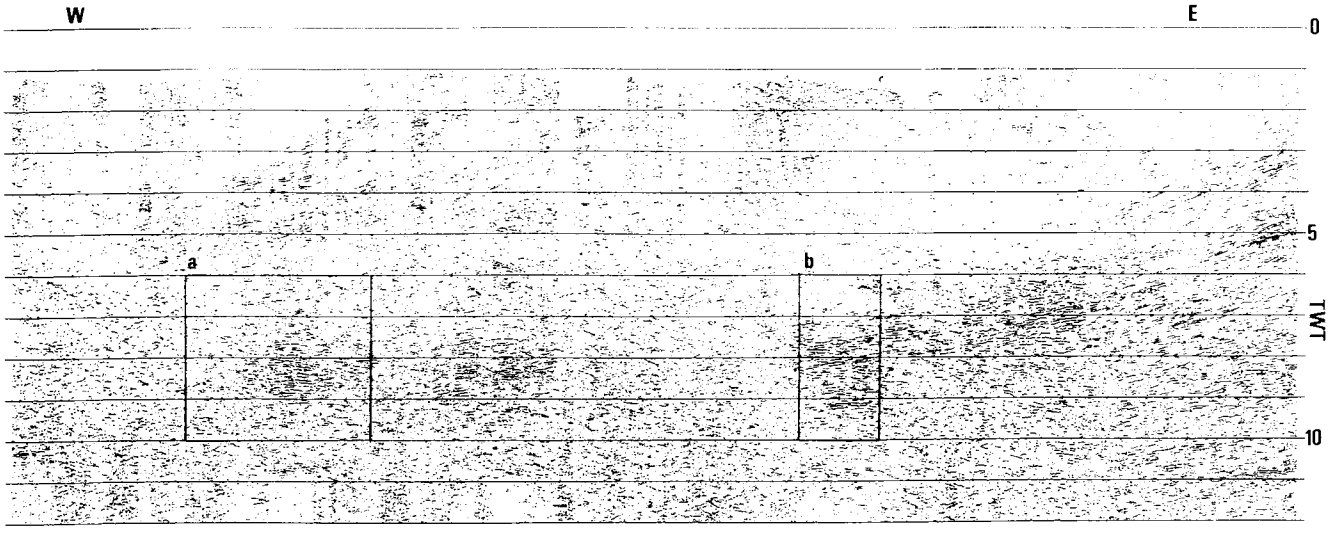

Figure 18. True relative amplitude stack section of LITHOPROBE Line 10. Processing steps described in text. The boxes *a* and *b* are shown in more detail in Fig. 20.

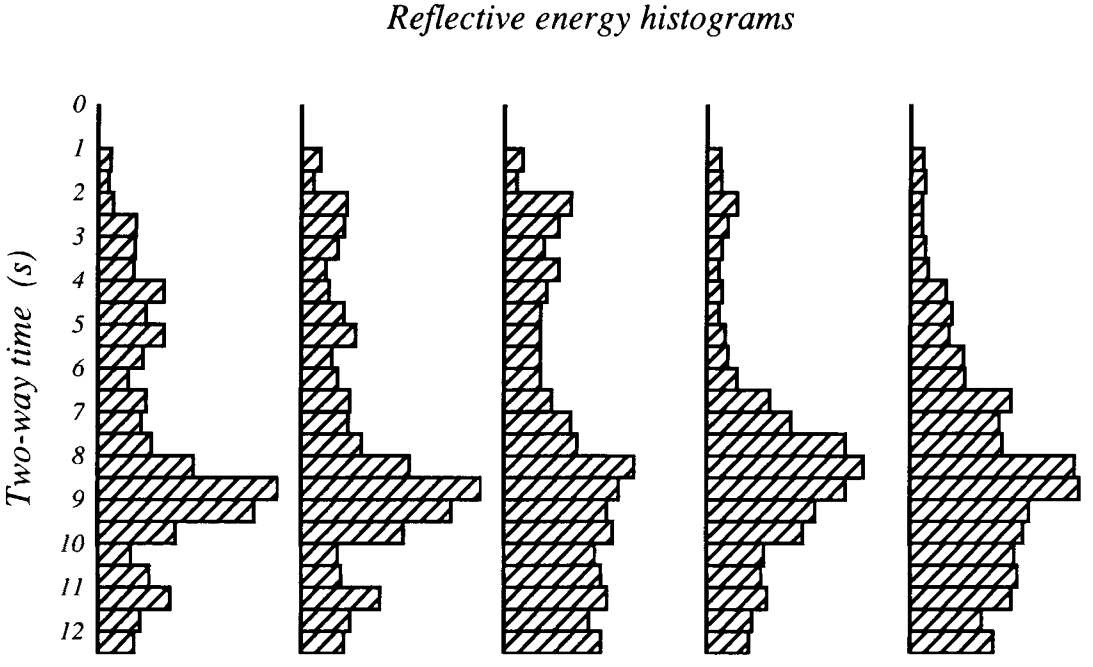

Figure 19. Reflectivity energy histograms of the true relative amplitude section of LITHOPROBE Line 10. Note the shallowing of the increased reflectivity from west to east.

lower crust occurs at 400–450 °C (e.g. Jones 1987; Hyndman & Shearer 1989). We therefore have estimated the depths of this temperature along the profiles. There are no heat-flow measurements directly on LITHOPROBE Lines 9 and 10; the nearest values are 25–50 km to the north or south (Lewis *et al.* 1992). Thus it is not possible to define the thermal transition accurately across the profiles. We have calculated averages within one degree of longitude boxes to obtain a mean heat-flow profile (Fig. 21). It is clear that there is an important increase in heat flow from west to east. The thermal boundary appears to be located around 120°W.

In order to obtain an estimate of the temperature distribution at depth for both the Intermontane and Omineca belts, we have started from the assumption that they are part of the same heat-flow province, and thus the heat-flow differences result from differences in average crustal heat generation. The average heat flow and surface-heat generation for the Intermontane belt are both quite uniform, 72.6 mW m^{-2} and 1.2 μW m^{-3} respectively. For the whole Omineca Belt these values show much more variation with averages of 86.3 mW m^{-2} and 4.0 μW m^{-3}. There is more extensive heat generation than heat-flow data, so we have used the mean heat generation as being more representative, and have obtained the depths to the 450 °C

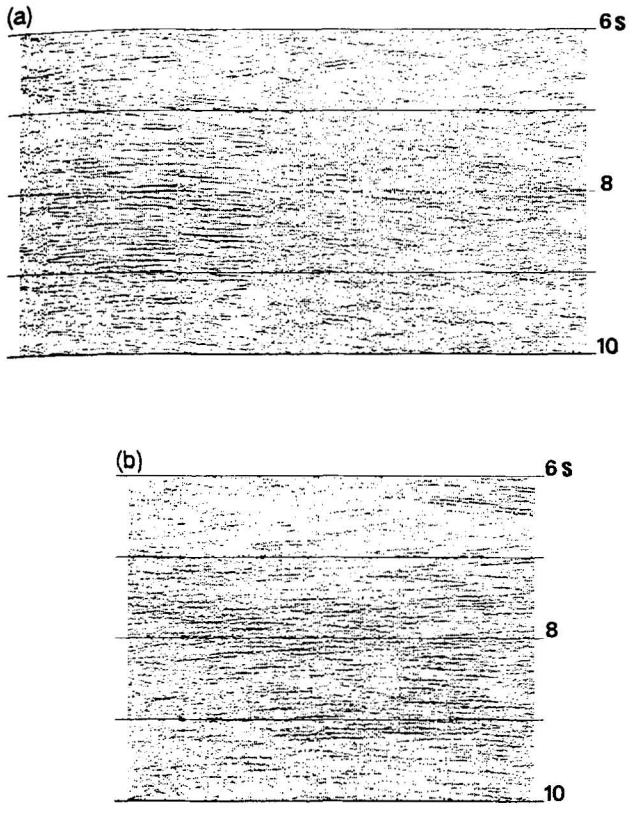

Figure 20. Details from the section shown in Fig. 18, showing examples of reflector geometry in the highly reflective zones.

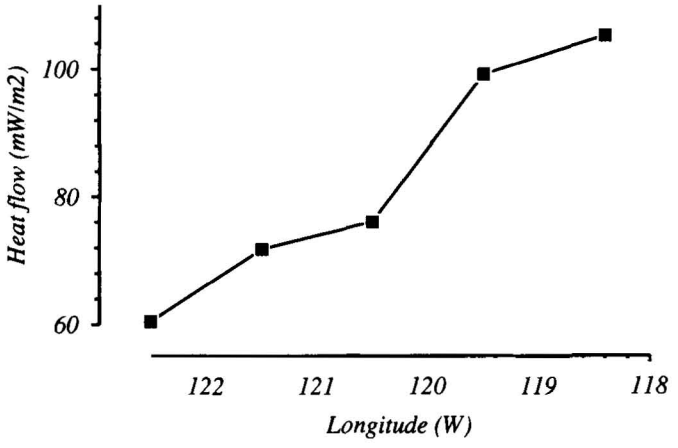

Figure 21. Synthetic heat-flow profile made of local averages (one degree of longitude boxes) of the geothermal data compilation of Lewis *et al.* (1992). There is an important variation in heat flow around 120°W, the approximate location of the Intermontane–Omineca boundary.

isotherms from the work of Majorowicz, Gough & Lewis (1993). The 450 °C temperatures are estimated to occur at about 15–18 km for the Intermontane Belt and 10–12 km for the Omineca Belt. Although there is an uncertainty of about ±3 km in these depths, the difference between the Intermontane and Omineca belt thermal regimes is clearly significant, and the values close to the depth to the conductive layer across both belts.

DISCUSSION

Structure at the Intermontane–Omineca boundary and lithospheric evolution

The simplified cross-section of Fig. 22 shows the horizontal transition in the mid-crust of electrical conductivity, seismic reflectivity and mid-crustal temperatures in the region of the Okanagan Valley. The Okanagan Valley Fault (OVF) is interpreted, from geological mapping and guided by the seismic-reflection data, to be dipping shallowly westward. Its most recent activity appears to have been as a normal fault associated with Eocene extension. However, it probably also accommodated earlier crustal shortening which carried a series of terranes eastward on top of ancestral North America. The origin of the rocks below the OVF cannot be determined with confidence from the seismic data. Cook *et al.* (1992; see Fig. 17) preferred allochthonous exotic terrane rocks above and below the fault, with ancestral North American rocks at greater depth. However, our analyses of the MT data show that a pronounced change in strike occurs at depths of about 10 km right across the Okanagan Valley. Furthermore, our modelling studies show that at these depths there is a significant decrease in electrical resistivity (increase in electrical conductivity). Thus, we interpret the allochthonous terranes to be only of the order of 10 km thick (Fig. 23). A detachment surface at this depth is in agreement with thermal-rheological models by Lowe & Ranalli (1993), who imply such a depth of minimum strength for this region during the shortening period. The Eocene extension normal faulting, which has modest displacements, may have affected a somewhat greater depth. The deeper crust consists of North American rocks. Geometrical considerations imply that if this is the case, then the Nicola Horst should be cored by North American rocks, not allochthonous exotic ones (Cook, personal communication, 1993).

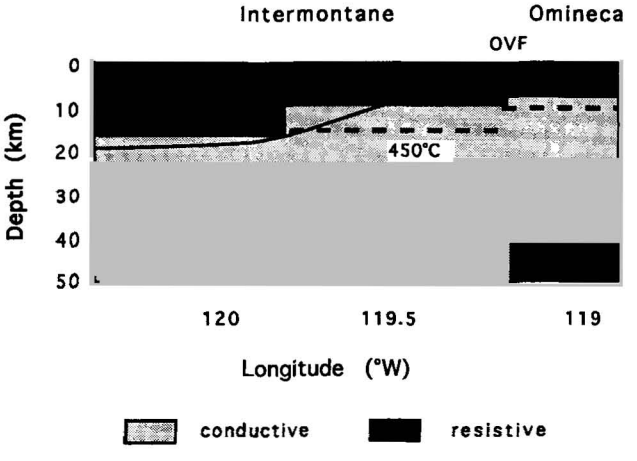

Figure 22. Synthesis figure showing the mid to lower crustal conductive layer, the 450 °C isotherms. Note the difference in resistivity above and below the Okanagan Valley Fault (OVF), as well as the near coincidence of the low-resistivity layer, the 450 °C isotherm and the depth of the OVF (corresponding to the top of the reflective layer in Fig. 18).

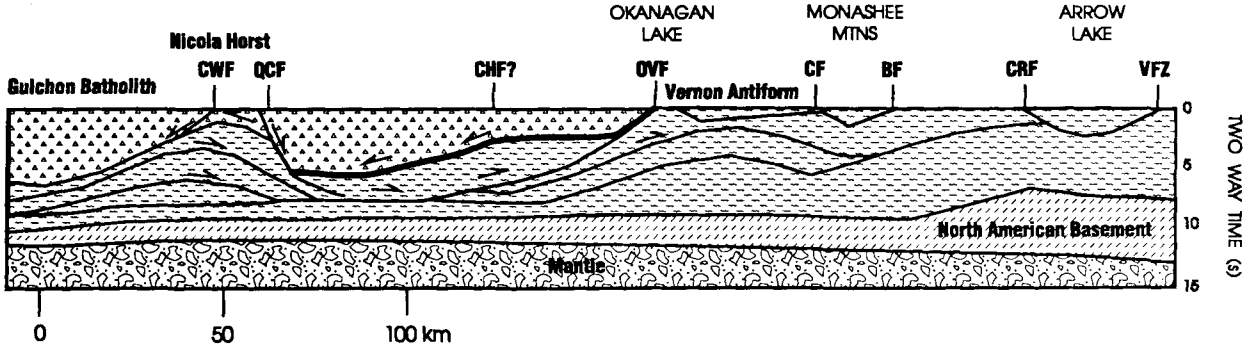

Figure 23. Revised interpretation of the crustal structure across the Intermontane–Omineca boundary incorporating the results presented in this paper. Shading patterns and symbols same as Fig. 17.

Interpretation of combined geophysical data for the lower crust

Our analyses show that there is good agreement, within the recognized uncertainties, between the depth to the top of the conductive and reflective layers in both the Intermontane and Omineca belts. The change occurs in approximately the same location near the Okanagan Valley. There is also good agreement between their tops and the 400–450 °C isotherm. The agreement in depth in this well-studied area supports the general agreement from global compilations (e.g. Hyndman & Shearer 1989; Marquis & Hyndman 1992). In the absence of any other information, taking the simplest possible interpretation this agreement suggests that the conductive and reflective layers may have a common origin. Other constraints on the origin are: that the high conductivity and reflectivity in the deep crust are continued across major boundaries in the surface structure, and that the tops are at about 400–450 °C (see Hyndman *et al.* 1993, for a discussion of these constraints from global data).

The debate on the origin of the frequently observed deep crustal high conductivity has been primarily between saline fluid porosity and thin films of graphite (or other metallic phase). The most commonly accepted explanations for the deep crustal reflectivity have been layered mafic intrusions and horizontal mylonite shear zones. Layered horizontal porosity has also been suggested, but this is not widely accepted in the seismic-reflection community. If conductivity and reflectivity indeed have a common origin, this provides a very important constraint. Thin (graphite) films cannot significantly affect the seismic properties, and (dry) mafic layering cannot explain the high conductivity. The association of the tops with present temperatures of 400–450 °C also suggests that their origin is ephemeral; if the temperatures decline or increase, the boundary will deepen or shoal. The only common explanation that seems to meet these requirements is aqueous fluid porosity.

This thesis is not new. Matthews (1986) suggested fluids to explain the enhanced lower crustal reflectivity around the British Isles. Jones (1987) proposed that some of the frequently observed lower crustal conductors and reflectors might both be caused by fluids. Hyndman & Shearer (1989) and Marquis & Hyndman (1992) investigated the conditions under which fluids might be present, and the reader is referred to these papers for more details. Merzer & Klemperer (1992) proposed discrete, highly conducting lamellae to explain both the observed reflectivity and the low electrical resistivity of the lower crust. The aforementioned studies were mostly of a conceptual nature: few direct local correlations were presented. Jones (1987) discussed such correlations for six nearly coincident MT and reflection studies, and Hyndman (1988) presented the case in detail of coincident conductors and reflectors at lower crustal depths in the special environment of the Cascadia subduction zone. More detailed seismic work done in that zone by Calvert & Clowes (1990) showed that the reflection coefficients of the so-called '*E*' reflector are best explained by fluids in a shear zone.

Fluids as the cause of reflectivity have already been suggested by Lewis *et al.* (1992) and Lewis, Bentkowski & Hyndman (1993) for the LITHOPROBE Southern Cordillera Transect, where they found a correlation of depth to the top of reflectivity with the 450 °C isotherms (brittle–ductile transition temperature). A similar case of high reflectivity following heat-flow pattern has been discussed by Hyndman, Lewis & Marquis (1991) for the Basin and Range Province. There the reflectors are shallower in the high-heat-flow Buena Vista Valley than in the low-heat-flow Grass Valley, with the onset of reflectivity near the 450 °C isotherm in both cases. Jones *et al.* (1992a) also pointed out, on the basis of coincident conductive and reflective layers in the LITHOPROBE Southern Cordillera transect, that some of the observed reflectors cannot be explained by structural changes, and suggested fluids as an explanation.

Trapping of fluids at lower crustal depths

Even though the conclusions above support the presence of fluids in the deepest crust, the question of how substantial amounts of fluids can be trapped at depth for geologically significant periods of time remains a very important problem. In a ductile lower crust, the porosity should be in minimum energy equilibrium pores (e.g. von Bargen & Waff 1986). Marquis & Hyndman (1992) proposed a mechanism to trap the fluids at depth invoking deformation of equilibrium pore geometries in lower crustal ductile shear zones. This might be the case in the region studied here because: the conductive/reflective layers are at temperatures above the brittle–ductile transition and the stress regime is compressive (Zoback 1992), implying continuous shearing at the brittle–ductile transition. Gough (1986b) had previously argued that the stress regime plays an important role in the

interconnectivity of deep crustal saline fluids, and Bailey (1990) showed theoretically that the brittle–ductile transition can form an impermeable barrier that can block upward migration of fluids.

This mechanism, that might be currently active in the Canadian Cordillera, may have been active in Alaska during Cretaceous–Palaeocene time. Goldfarb *et al.* (1991) present isotopic data from the Juneau Gold Belt supporting a rapid, widespread fluid release at 56–55 Ma, coinciding with a change in crustal stress regime. As long as the Kula plate motion remained orthogonal to subduction (from about 110 to 56 Ma), the fluids remained trapped. They were released when the motion shifted to oblique subduction at 56 Ma. The large horizontal stresses capped the porosity right under the brittle–ductile transition. The fluids were released rapidly following a reduction in horizontal stress associated to the change in plate motion.

CONCLUSIONS

State-of-the-art processing and analysis of high-quality MT data and reprocessing of collocated multichannel seismic-reflection data reveal a zone of low electrical resistivity and high seismic reflectivity in the deep crust of the Intermontane Belt and the western portion of the Omineca Belt. The tops to both anomalous features follow the heat-flow pattern in the area; the layers being shallower with increasing heat flow. One explanation for both features of the middle crust is the presence of small amount of saline fluid trapped in a deep crustal shear zone under the brittle–ductile transition.

In addition, we have demonstrated a depth dependency in strike, with the uppermost crust (5–10 km) striking N25°W, the rest of the crust striking N20°E, and the upper mantle striking N60°E. This implies a major horizontal boundary and that only the upper 5 to 10 km of the crust is made of exotic material; the bulk of the crust consists of ancient North American rocks.

ACKNOWLEDGMENTS

The MT data were acquired by Phoenix Geophysics (Toronto) Ltd, and the seismic-reflection data were recorded by Sonix Ltd and initial processing was performed by Western Geophysical Ltd. Thanks to John Weaver and Ashok Agarwal, and to Torquil Smith and John Booker, for their MT-inversion programs, and to Kris Vasudevan and Rolf Maier for their help at the LITHOPROBE Seismic Processing Facility in Calgary. Torquil Smith is especially thanked for providing a version of his code that derived the same static-shift factors for each mode so that we could derive the applicable site gains. Reviews by Dave Eaton, Randy Parrish, and two anonymous referees greatly helped in improving this paper. Funding for this work was provided by a LITHOPROBE Grant to RDH and a Science Council of British Columbia GREAT Award to GM.

This paper is Geological Survey of Canada Contribution Number 26694 and LITHOPROBE Contribution number 590.

REFERENCES

Agarwal, A.K., Poll, H.E. & Weaver, J.T., 1993. One and two-dimensional inversion of MT data in continental regions, *Phys. Earth planet. Inter.*, **81,** 155–176.

Bailey, R.C., 1990. Trapping of aqueous fluids in the deep crust, *Geophys. Res. Lett.*, **17,** 1129–1132.

Berdichevsky, M.N. & Dmitriev, V.I., 1976. Basic principles of interpretation of magnetotelluric sounding curves, in *Geoelectric and geothermal studies,* pp. 165–221, ed. Adam, A., Akademiai Kiado, Budapest.

Berdichevsky, M.N., Vanyan, L.L. & Dmitriev, V.I., 1989. Methods used in the USSR to reduce near-surface inhomogeneity effects on deep magnetotelluric sounding, *Phys. Earth planet. Inter.*, **53,** 194–206.

Bittner, R. & Wever, Th., 1991. Energy histograms for the characterization of deep reflection seismic profiles, *Geophys. J. Int.*, **105,** 37–43.

Booker, J.R. & Chave, A.D., 1989. Introduction to the Special Section on the EMSLAB-Juan de Fuca Experiment. *J. geophys. Res.*, **94,** 14 093–14 098.

Calvert, A.J. & Clowes, R.M., 1990. Deep, high-amplitude reflections from a major shear zone above the subducting Juan de Fuca plate, *Geology,* **18,** 1091–1094.

Caner, B., 1970. Electrical conductivity structure in western Canada and petrological implications. *J. Geomagn. Geoelect.*, **22,** 113–129.

Caner, B., 1971. Quantitative interpretation of geomagnetic depth sounding data in western Canada, *J. geophys. Res.*, **76,** 7202–7216.

Caner, B. & Cannon, W.H., 1965. Geomagnetic depth-sounding and correlation with other geophysical data in western North America, *Nature,* **207,** 927–929.

Caner, B., Camfield, P.A., Andersen, F. & Niblett, E.R., 1969. A large-scale magnetotelluric survey in western Canada, *Can. J. Earth. Sci.*, **6,** 1245–1261.

Cook, F.A., Varsek, J.L. & Clowes, R.M., 1991. LITHOPROBE reflection transect of southwestern Canada: Mesozoic Thrust and Fold Belt to mid-ocean ridge, in *Continental Lithosphere: Deep Seismic Reflections,* pp. 247–255, eds Meissner, R., Brown, L., Durbaum, H.J., Franke, W., Fuchs, K. & Siefert, F., Geodyn. Ser. Vol. 22, Am. Geophys. Un., Washington, DC.

Cook, F.A., Varsek, J.L., Clowes, R.M., Kanasewich, E.R., Spencer, C., Parrish, R.R., Brown, R.L., Carr, S.D., Johnson, B.J. & Price, R.A., 1992. LITHOPROBE crustal reflection cross section of the southern Canadian Cordillera I: Foreland Thrust and Fold Belt to Fraser River Fault, *Tectonics,* **11,** 12–35.

deGroot-Hedlin, C., 1991. Removal of static shift in two dimensions by regularized inversion, *Geophysics,* **56,** 2102–2106.

EMSLAB Group, 1988. The EMSLAB electromagnetic sounding experiment, *EOS, Trans. Am. geophys. Un.,* **69,** 89 & 98–99.

Gabrielse, H. & Yorath, C.J., 1991. Introduction, in *Geology of the Cordilleran Orogen in Canada,* pp. 15–59, eds Gabrielse, H. & Yorath, C.J., Geology of North America, Vol. G-2, Geol. Soc. Am., Geol. Surv. Can., Ottawa.

Gamble, T.D., Goubau, W.M. & Clarke, J., 1979. Magnetotellurics with a remote reference, *Geophysics,* **44,** 53–68.

Goldfarb, R.J., Snee, L.W., Miller, L.D. & Newberry, R.J., 1991. Rapid dewatering of the crust deduced from ages of mesothermal gold deposits, *Nature,* **354,** 296–298.

Gough, D.I., 1986a. Mantle upflow tectonics and the Canadian Cordillera, *J. geophys. Res.*, **91,** 1909–1919.

Gough, D.I., 1986b. Seismic reflectors, conductivity, water and stress in the lower continental crust, *Nature,* **323,** 143–144.

Gough, D.I. & Majorowicz, J.A., 1992. Magnetotelluric soundings, structure, and fluids in the southern Canadian Cordillera, *Can. J. Earth Sci.*, **29,** 609–620.

Gough, D.I., Bingham, D.K., Ingham, M.R. & Alabi, A.O., 1982.

Conductive structures in southern Canada: a regional magnetometer array study, *Can. J. Earth Sci.*, **19,** 1680–1690.

Gough, D.I., McKirdy, D.McN., Woods, D.V. & Geiger, H., 1989. Conductive structures and tectonics beneath the EMSLAB land array, *J. geophys. Res.*, **94,** 14 099–14 110.

Groom, R.W. & Bailey, R.C., 1989. Decomposition of magnetotelluric impedance tensors in the presence of local three-dimensional galvanic distortion, *J. geophys. Res.*, **94,** 1913–1925.

Groom, R.W. & Bailey, R.C., 1991. Analytic investigations on the effects of near-surface three-dimensional galvanic scatterers on MT tensor decompositions, *Geophysics*, **56,** 496–518.

Groom, R. W., Kurtz, R.D., Jones, A.G. & Boerner, D.E., 1993. A quantitative methodology to extract regional magnetotelluric impedances and determine the dimension of the conductivity, *Geophys. J. Int.*, **115,** 1095–1118.

Haak, V. & Hutton, V.R.S., 1986. Electrical resistivity in continental lower crust, in *The Nature of the Lower Continental Crust*, ed. J.B. Dawson, D.A. Carswell, J. Hall & Wedepohl, K.H., Geol. Soc. London, Spec. Publ., **24,** 35–49.

Hyndman, R.D., 1988. Dipping seismic reflectors, electrically conductive zones and trapped water in the crust over a subducting plate, *J. geophys. Res.*, **93,** 13 391–13 405.

Hyndman, R.D. & Hyndman, D.W., 1968. Water saturation and high electrical conductivity in the lower crust, *Earth planet. Sci. Lett.*, **4,** 427–432.

Hyndman, R.D. & Shearer, P.M., 1989. Water in the lower continental crust: modelling magnetotelluric and seismic reflection results, *Geophys. J. Int.*, **98,** 343–365.

Hyndman, R.D., Lewis, T.J. & Marquis, G., 1991. Comment on 'Origin of deep crustal reflections: implications of coincident refraction and reflection data in Nevada' by Holbrook, Catchings and Jarchow, *Geology*, **19,** 1243.

Hyndman, R.D., Vanyan, L.L., Marquis, G. & Law, L.K., 1993. The origin of electrically conductive lower continental crust: saline water or graphite? *Phys. Earth planet. Inter.*, **81,** 325–344.

Irving, E. & Wynne, P.J., 1991. Paleomagnetism: review and tectonic implications, in *Geology of the Cordilleran Orogen in Canada*, pp. 61–86, eds Gabrielse, H. & Yorath, C.J., Geology of North America, Vol. G-2, Geol. Soc. Am., Geol. Surv. Can., Ottawa.

Jiracek, G.R., 1990. Near-surface and topographic distortions in electromagnetic induction, *Surv. Geophys.*, **11,** 163–203.

Jones, A.G., 1987. MT and reflection: an essential combination. *Geophys. J.R. astr. Soc.*, **89,** 7–18.

Jones, A.G., 1988. Static shift of magnetotelluric data and its removal in a sedimentary basin environment, *Geophysics*, **53,** 967–978.

Jones, A.G., 1992. Electrical conductivity of the continental lower crust, in *Continental Lower Crust*, pp. 81–143, eds Fountain, D.M., Arculus, R. & Kay, R.W., Elsevier, Amsterdam.

Jones, A.G. & Groom, R.W., 1993. Strike angle determination from the magnetotelluric impedance tensor in the presence of noise and local distortion: Rotate at your peril!, *Geophys. J. Int.*, **113,** 524–534.

Jones, A.G., Groom, R.W. & Kurtz, R.D., 1993. Decomposition and modelling of the BC87 dataset, *J. Geomagn. Geoelect.*, **45,** 1127–1150.

Jones, A.G., Chave, A.D., Egbert, G., Auld, D. & Bahr, K., 1989. A comparison of techniques for magnetotelluric response function estimation, *J. geophys. Res.*, **94,** 14 201–14 213.

Jones, A.G., Kurtz, R.D., Oldenburg, D.W., Boerner, D.E. & Ellis, R., 1988. Magnetotelluric observations along the LITHOPROBE southeastern Canadian Cordilleran transect, *Geophys. Res. Lett.*, **15,** 677–680.

Jones, A.G., Kurtz, R.D., Boerner, D.E., Craven, J.A., McNeice, G., Gough, D.I. & DeLaurier, J.M., 1990. Electromagnetic investigations over the southern Cordilleran Lithoprobe transect: 1990 status report, Extended Abstr., in *Lithoprobe Cordilleran Workshop 1990*, pp. 64–74, Lithoprobe Report No. 11, Lithoprobe Secretariat, University of British Columbia, Vancouver.

Jones, A.G., Gough, D.I., Kurtz, R.D., DeLaurier, J.M., Boerner, D.E., Craven, J.A., Ellis, R.G., & McNeice, G.W., 1992a. Electromagnetic images of regional structure in the southern Canadian Cordillera, *Geophys. Res., Lett.*, **12,** 2373–2376.

Jones, A.G., Kurtz, R.D., Boerner, D.E., Craven, J.A., McNeice, G., Gough, D.I., DeLaurier, J.M. & Ellis, R.G., 1991. Electromagnetic investigations over the southern Cordilleran Lithoprobe transect: 1991 status report, Extended Abstr., in *Lithoprobe Cordilleran Workshop 1991*, pp. 38–55, Lithoprobe Report No. 16, Lithoprobe Secretariat, University of British Columbia, Vancouver.

Kaufman, A.A. & Keller, G.V., 1981. *The Magnetotelluric Sounding Method*, Elsevier, Amsterdam.

Kurtz, R.D., DeLaurier, J.M. & Gupta, J.C., 1990. The electrical conductivity distribution beneath Vancouver Island: a region of active plate subduction, *J. geophys. Res.*, **95,** 10 929–10 946.

Lewis, T.J., Bentkowski, W.H. & Hyndman, R.D., 1992. Crustal temperatures near the LITHOPROBE Southern Canadian Cordilleran Transect, *Can. J. Earth Sci.*, **29,** 1197–1124.

Lewis, T.J., Bentkowski, W.H. & Hyndman, R.D., 1993. Crustal reflectors, metamorphic reactions and crustal temperatures in the Southern Canadian Cordillera, *Tectonophysics*, **225,** 57–61.

Lowe, C. & Ranalli, G., 1993. Density, temperature, and rheological models for the southeastern Canadian Cordillera: implications for its geodynamic evolution, *Can. J. Earth Sci.*, **30,** 77–93.

Majorowicz, J.A. & Gough, D.I., 1991. Crustal structures from MT soundings in the Canadian Cordillera, *Earth planet. Sci. Lett.*, **102,** 444–454.

Majorowicz, J.A., Gough, D.I. & Lewis, T.J., 1993. Correlation between the depth to the lower-crustal high conductive layer and heat flow in the Canadian Cordillera, *Tectonophysics*, **225,** 49–56.

Marquis, G. & Hyndman, R.D., 1992. Geophysical support for aqueous fluids in the deep crust: seismic and electrical relationships, *Geophys. J. Int.*, **110,** 91–105.

Matthews, D.H., 1986. Seismic reflections from the lower crust around Britain, in *The Nature of the Lower Continental Crust*, pp. 11–22, eds Dawson, J.B., Carswell, D.A., Hall, J. & Wedepohl, K.H., Spec. Publ. 24, Geol. Soc. London.

Merzer, A.M. & Klemperer, S.L., 1992. High electrical conductivity in a model lower crust with unconnected, conductive, seismically reflective layers, *Geophys. J. Int.*, **108,** 895–905.

Milkereit, B. & Spencer, C., 1989. Noise suppression and coherency enhancement of seismic data, in *Statistical applications in the earth sciences*, pp. 243–248, eds Agterberg, F.P. & Bonham-Carter, G.F., Paper 89-9, Geol. Surv. Can., Ottawa.

Olhoeft, G.R., 1981. Electrical properties of granite with implications for the lower crust, *J. geophys. Res.*, **86,** 931–936.

Poll, H.E., Weaver, J.T. & Jones, A.G., 1989. Calculations of voltages for magnetotelluric modelling of a region with near-surface inhomogeneities, *Phys. Earth planet. Inter.*, **53,** 287–297.

Smith, J.T. & Booker, J.R., 1991. Rapid inversion of two and three-dimensional magnetotelluric data. *J. geophys. Res.*, **96,** 3905–3922.

Sternberg, B.K., Washburne, J.C. & Pellerin, L., 1988. Correction for the static shift in magnetotellurics using transient electromagnetic soundings. *Geophysics*, **53,** 1459–1468.

Stesky, R.M. & Brace, W.F., 1978. Electrical conductivity of serpentinized rocks to 6 kilobars, *J. geophys. Res.*, **41,** 529–547.

von Bargen, N. & Waff, H.S., 1986. Permeabilities, interfacial areas and curvatures of partially molten systems: results of numerical

computations of equilibrium microstructures, *J. geophys. Res.*, **91,** 9261–9276.

Vozoff, K., (ed.), 1986. *Magnetotelluric Methods,* Soc. Expl. Geophys. Reprint Ser. No. 5, Soc. Expl. Geophys., Tulsa, OK.

Weaver, J.T. & Agarwal, A.K., 1992. Automatic one-dimensional inversion of magnetotelluric data by the method of modelling, *Geophys. J. Int.*, **112,** 115–123.

Wight, D.E., Bostick, F.X. & Smith, H.W., 1977. *Real-time Fourier transformation of magnetotelluric data,* Unpubl. report, Electrical Geophys. Res. Lab., University of Texas, Austin, TX.

Zoback, M.L., 1992. First and second-order patterns of stress in the lithosphere: the World Stress Map project, *J. geophys. Res.*, **97,** 11 703–11 728.